UNIVERSITY OF CALIFORNIA,
IRVINE

Human immunodeficiency virus evolutionary dynamics in compartmentalised settings: a mathematical & computational approach

DISSERTATION

submitted in partial satisfaction of the requirements
for the degree of

DOCTOR OF PHILOSOPHY

in Computational Science

by

Wen-Jian Chung

Dissertation Committee:
Professor Dominik Franz Xavier Wodarz, Chair
Professor Ricardo Carretero–Gonzalez
Professor Forest Rohwer
Associate Professor Elizabeth Read
Assistant Professor Daniel Parker

2023

DEDICATION

To my grandmother Lean Choo Oh, who passed away one year before the completion of this work and is dearly missed, and to my family, parents Chok Yin Chung and Li Sim Chuah, and sister Wei-Lyn Chung who have supported me with their love and care throughout these long years.

TABLE OF CONTENTS

LIST OF FIGURES

LIST OF TABLES

ACKNOWLEDGMENTS

I would like to thank Prof. Dominik Wodarz and Prof. Ricardo Carretero–Gonzalez for their support and mentorship over the course of this PhD, Prof. Forest Rohwer for his advice and willing participation as a committee member, and Prof. Elizabeth Read and Prof. Daniel Parker for also being willing to serve on my committee. I would also like to thank Prof. Virginia Trimble and Prof. Joseph Mahaffy for their encouragement, advice, and moral support.

VITA

Wen-Jian Chung

EDUCATION

Doctor of Philosophy in Computational Sciences — **2023**
University of California, Irvine — *Irvine, California*
(joint program with San Diego State University)

Master of Science in Physics — **2007**
Bishop's University — *Lennoxville, Quebec*

Bachelor of Science in Physics — **2007**
University of Toronto — *Toronto, Ontario*

RESEARCH EXPERIENCE

Graduate Research Assistant — **2019–2023**
University of California, Irvine — *Irvine, California*

Graduate Research Assistant — **2018–2019**
San Diego State University — *San Diego, California*

Graduate Research Assistant — **2013–2016**
Bishop's University — *Lennoxville, Quebec*

TEACHING EXPERIENCE

Teaching Assistant — **2019–2022**
University of California, Irvine — *Irvine, California*

Teaching Assistant — **2018–2019**
San Diego State University — *San Diego, California*

Teaching Assistant — **2014–2016**
Bishop's University — *Lennoxville, Quebec*

REFEREED JOURNAL PUBLICATIONS

Bose-Einstein condensate & degenerate Fermi cored dark matter halos **2016**
Journal of Cosmology & Astrophysics

Simultaneous baldness and cosmic baldness and the Kottler spacetime **2018**
Physical Review D

Human immunodeficiency virus (HIV) dynamics in secondary lymphoid tissues and the evolution of cytotoxic T lymphocyte (CTL) escape mutants **2023**
Virus Evolution

ABSTRACT OF THE DISSERTATION

Human immunodeficiency virus evolutionary dynamics in compartmentalised settings: a mathematical & computational approach

By

Wen-Jian Chung

Doctor of Philosophy in Computational Science

University of California, Irvine, 2023

Professor Dominik Franz Xavier Wodarz, Chair

Experimental observations indicate that the human immunodeficiency virus (HIV) can replicate in both the follicular and extrafollicular parts of secondary lymphoid tissues, HIV's primary replication site. The former is an immune privileged zone with low cytotoxic lymphocyte activity, and thus HIV replication is primarily concentrated there. Mathematical models and stochastic Gillespie simulations show that this compartmentalization potentially explains several seemingly counterintuitive observations. First, the observation of post-therapy viral decline rate's independence of cytotoxic T-lymphocyte (CTL) presence in simian immunodeficiency virus (SIV)-infected macaques, assuming CTL-mediated lysis significantly contributes to viral suppression. Second, the slow emergence of CTL-escape mutants during chronic infection even if CTL-mediated lysis is responsible for viral suppression. Heterogeneity in CTL activity, and consequently the selection pressure and infected cell population sizes, between the follicular and extrafollicular compartments can explain these findings. The effect of secondary lymphoid tissue compartmentalization is also examined in the context of non-escape scenarios, where the mutant HIV strain is recognised by the CTL response. These findings highlight the importance of measuring viral populations separately in the extrafollicular and follicular compartments; peripheral blood viral load hides the heterogeneity between compartments and its potential effects.

Chapter 1

Introduction

The original motivation behind the work in this dissertation is to propose another explanation for the observed phenomenon of slow immune escape: compartmentalisation within the human body, particularly in lymphoid tissues, and the presence of immune privileged "safe havens" for the human immunodeficiency virus (HIV) may also play an important role in the evolutionary dynamics of HIV in general. It is noteworthy that most mathematical models of HIV treat the body as one homogeneous medium in which HIV infection takes place. However, the human body is anything but homogeneous, consisting of many different types of tissue with a lot of barriers between. HIV replication mostly takes place in secondary lymphoid tissues such as the lymph nodes, spleen, or gut-associated lymphoid tissue. Within these tissues, viral replication tends to be concentrated in B cell follicles, with lower levels of replication observed in the extrafollicular compartments. One reason for this is that the follicular compartment contains follicular CD4+ helper T-cells that are more permissive to HIV than those in the extrafollicular compartment. The presence of a high concentration of extracellular virions on the surface of follicular dendritic cells (FDCs) can also contribute to viral spread in the follicular compartment. Furthermore, because CTLs have limited or no presence in these compartments, they constitute an immune-privileged zone like the

central nervous system or testes. These zones can become "safe havens" where HIV is able to replicate relatively undisturbed by the immune response.

Using two-compartment deterministic ordinary differential equation (ODE) mathematical models building on the basic dynamics established in this introduction and computational stochastic simulations and comparing them with simpler single-compartment models, one of the goals of this dissertation is to show that the permeability of these follicular reservoirs to both infected cells and CTLs can significantly affect the amount of time it takes for HIV to evolve an escape to the immune response. This can be intuitively explained by the fact that the reservoirs in the follicular tissue where CTL activity is limited become safe havens, thus the selective pressure on HIV to evolve an escape to the immune response is much lower there. This is especially true if there is a cost to viral replication or infectiousness that has been usually associated with such mutations. Since the majority of the HIV replication will be occurring in the follicular compartment, and not in the extrafollicular compartment where the CTL response is much stronger and thus better able to control HIV replication, it will take much longer for an escape strain that has worse infectiousness or replication rate to emerge and take hold in the entire system due to the lower selective pressure from CTLs in the follicular compartment. However, the compartmentalisation of lymphoid tissues also has other important effects on HIV dynamics, and the dissertation also covers the extended work.

This dissertation is structured into five main chapters. The first chapter will provide background on HIV, basic mathematical models of HIV dynamics, and secondary lymphoid tissues in order to provide context for the main body of work in the following chapters. The immunology of HIV infection in secondary lymphoid tissues is a highly complex subject that could be the subject of multiple dissertations; regrettably, in the interests of brevity, the author will only be able to cover the aspects relevant to the work in this dissertation.

The second chapter primarily concentrates on studying the effect of lymphoid tissue com-

partmentalisation on HIV dynamics using deterministic ODE models. One particularly important effect studied here is that which compartmentalisation has on HIV decline with the application of anti-retroviral therapy (ART). Experimental observations have established that the rate of decline in infected cell populations (and thus infected cell lifetime) following ART is remarkably consistent, irrespective of disease stage or the amount of immune control. This observation was confirmed by Klatt et al. in the SIV lab model by comparing control simian subjects, where the CTL response is robust, with CTL-depleted monkeys, where there is no CTL response. In both cases, the rate of decline in the viral load after ART initiation was identical. From this result, they concluded that CTLs do not kill but suppress infected cells by non-lytic means. However, lymphoid tissue compartmentalisation and low CTL action in the immune-privileged follicular compartment may provide an alternative explanation. This chapter also provides some of the theoretical background for the two-compartment ODE models, which form the basis for the two-compartment stochastic models used in the following chapter.

The third chapter moves on to using a stochastic modeling approach to simulate HIV CTL escape in compartmentalised lymphoid tissues. the process of HIV evolving an escape towards the immune response via mutation is fundamentally random and probabilistic due to the random nature of genetic mutations due to errors in ribonucleic acid (RNA) replication and transcription during the HIV replication process. It is therefore not completely appropriate to model the emergence of mutants using deterministic differential equations and it is therefore necessary to transition towards using *stochastic* simulations. In particular, for small populations, population fluctuations can sometimes lead to situations where population extinction occurs where a deterministic model might predict otherwise. Even with high viral loads (populations), stochastic effects can be important. The well-known Gillespie stochastic simulation algorithm, which originated from the study of chemical reactions is primarily used in this chapter. Some background and theory behind the Gillespie algorithm and its applicability to viral dynamics will also be discussed in this chapter. Two different

types of CTL escape are considered as well: one where the wild type can immediately jump to a complete escape from the CTL response, and one where the virus must first evolve some degree of escape from the CTL response before then evolving a complete escape. In both scenarios, it will be shown that increasing the degree of compartmentalisation between the follicular and extrafollicular compartments will greatly increase the time taken for a complete escape to the CTL response to evolve. This provides some support for the hypothesis that lymphoid tissue compartmentalisation can help explain why HIV is slow to evolve an escape to the host CTL response.

The fourth chapter further considers other effects of lymphoid tissue compartmentalisation on the evolutionary dynamics of HIV, Instead of only considering the evolution of CTL escape by HIV, which was concentrated on in the first two chapters, we will consider the evolution of mutants that do not escape the immune response, but whose mutations still have an impact on HIV's reproductive fitness. How does the compartmental structure of the lymphoid tissue influence the evolution of neutral, advantageous, or disadvantageous mutants? If we assume that the degree of exchange between the follicular and extrafollicular compartments is relatively small and the immune response is relatively strong, one compartment will have a small infected cell population and the other will have a significantly larger population. This considerably alters the evolutionary dynamics compared to those in a homogeneous single-compartment model. Both ODEs and stochastic approaches will be used to help gain a better understanding of the differences between a compartmentalised and non-compartmentalised model.

Finally, the concluding chapter will summarise the work and discuss other potential impacts the compartmentalised structure of lymphoid tissue could have on HIV's evolutionary dynamics in other contexts. Potential directions for future work will also be discussed.

It is important to emphasize that the compartmentalisation of lymphoid tissue is by no means mutually exclusive with the other explanations that have been proposed for HIV's

slow immune escape or the other phenomena examined; rather, it should be considered as contributing towards a more holistic picture of HIV's evolutionary dynamics in vivo.

Chapter 2

Background

2.1 HIV

HIV is a single-stranded enveloped RNA virus, a member of the Lentivirus genus of retroviruses. The basic structure of a HIV virion is illustrated in Fig. 2.1. It is a lymphtropic virus that primarily infects and kills CD4+ helper T-lymphocytes, which are critical in coordinating the adaptive immune response. However HIV is also capable of infecting other CD4-expressing immune cells such as macrophages and microglia. It is transmitted via infected bodily fluids, particularly blood and semen (1; 2).

The replication cycle of HIV is illustrated in Fig. 2.2. HIV first attaches to a CD4-expressing cell with its spike using gp120 envelope glycoprotein to bind to the CD4 and a chemokine coreceptor (CCR5 or CXCR4, depending on the strain). This initiates the fusion of the HIV envelope with the cell membrane, allowing the capsid containing the RNA to enter the cell. Once inside the cell, the two strands of RNA are transcribed into DNA using reverse transcriptase as the capsid is transported to the cell's nucleus (reverse transcription). Inside the nucleus, the viral DNA is released from the capsid, then the viral integrase integrates

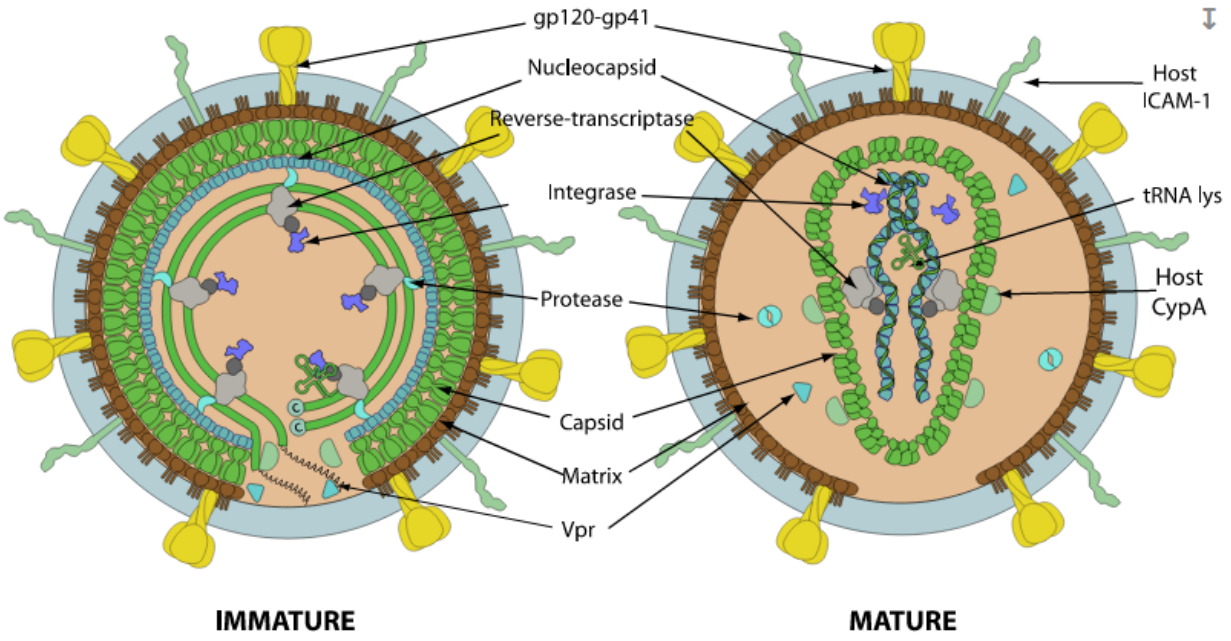

Figure 2.1: Structure of HIV-1 virions. Upon maturation, the capsid proteins form a bullet-shaped capsid surrounding the single-stranded RNA. The gp120 envelope glycoprotein attaches to CD4 receptors on immune cells and together with a coreceptor (CCR5 or CXCR4, depending on the HIV strain) facilitates HIV's entry into cell. (ViralZone (1))

the the viral genome into the host cell's own genome. This is a defining characteristic of retroviruses such as HIV. Once bound to the cell's DNA, the HIV DNA can either become dormant or activated to begin producing new HIV virions (1; 2).

Although HIV was only discovered in 1983, it is believed that HIV first infected humans via a zoonotic event (or events) that occurred in southern Cameroon sometime in the early 20th century. HIV-1, the most globally prevalent HIV subtype, is descended from the simian immunodeficiency virus (SIV), specifically the SIV subtype endemic in chimpanzees, SIVcpz. Because of the close similarities between SIV and HIV and the problematic ethics of performing HIV experiments with humans, SIV infection in primates such as macaques is often used as an experimental model for HIV infection in humans, such as in Connick et al. (2014) (3).

HIV infection is characterised by an initial acute infection followed by a long asymptomatic (clinically latent) phase. However, even during this clinical latent phase where there is lit-

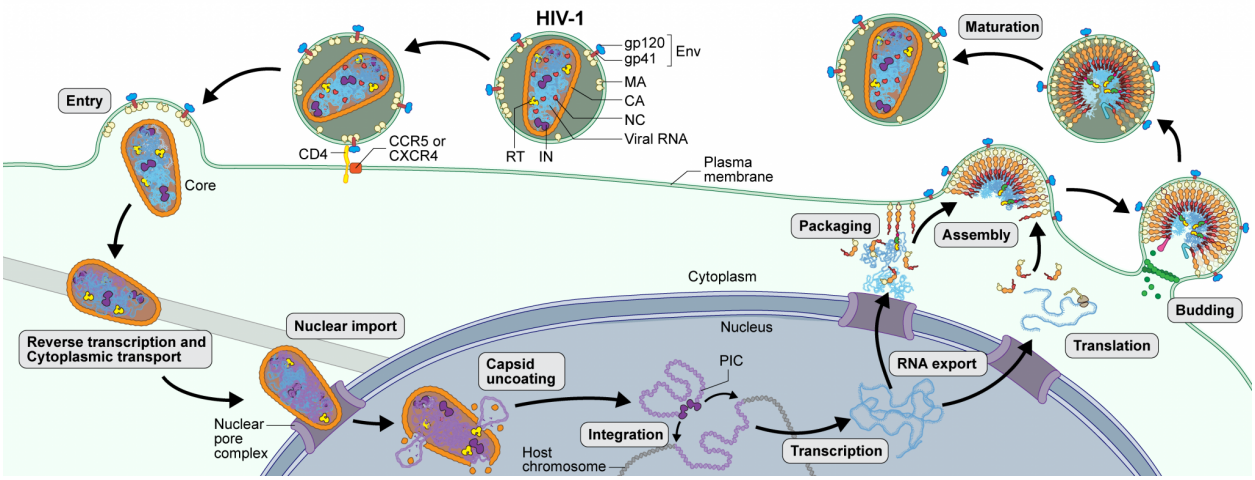

Figure 2.2: HIV replication cycle. (The Science of HIV Project (2))

tle, if any, detectable viremia, HIV is very much still actively replicating in the lymphoid tissues. As might be guessed from the name "lymphocyte", the lymphatic system contains 98% of an adult human body's lymphocytes. This means that even though HIV is primarily transmitted through infected blood or semen, it is actually in lymphoid tissues such as the spleen, lymph nodes, or gut-associated lymphoid tissue where the majority of HIV replication takes place. Eventually, without treatment to suppress HIV replication, immune exhaustion from persistent HIV infection results in the collapse of the adaptive immune response following HIV infection, which may occur up to 10 years after the initial infection. This is known as acquired immunodeficiency syndrome (AIDS), which is almost always fatal without treatment.

Due to the immense clinical impact that HIV infection and AIDS has had since the first AIDS cases were reported in 1981, the interaction between HIV and the human immune system has been the subject of intensive study. It is known that the human body quickly activates antibodies and cytotoxic CD8+ T-lymphocytes (CTLs) during the first phase of acute HIV infection, accompanied by a significant drop in the measured blood viral load. Yet HIV is usually able to survive this first response and establish itself in its host. The persistence of HIV in the human body despite the adaptive immune response has been attributed to

several factors. One of these is the fact that HIV has a very high replication rate, with some 10^{10}—10^{12} virions generated every day in the absence of antiretroviral therapy (ART), as well as a high mutation rate of approximately 3×10^{-5} per nucleotide base per replication cycle, thanks to the error-prone nature of RNA viral replication. This allows it to change the epitopes (the parts of the HIV antigen recognised by the immune system) that are normally targeted by both the humoral and cell-mediated immune responses, thus escaping the immune response (4). HIV is also able to establish itself in certain immune-privileged zones such as the brain or testicles, where it is able to reproduce unhindered (5; 6). HIV can also enter latency in infected cells: as a retrovirus, HIV's genome is integrated into the infected cell's own genome, where it can then be reactivated. During this latency period, no viral production takes place, and thus the infected cell is not targetable by the immune response (7).

Today, HIV infection is treatable with anti-retroviral therapy (ART) (9). However, there is no practical cure for HIV infection other than extremely dangerous procedures involving stem-cell/bone marrow transplants from donors with the CCR5-delta 32 mutation that confers resistance towards HIV infection, of which only five known successful cases exist (10). By contrast, according to the US government, some 38.4 million people lived with HIV worldwide in 2021 (11). While new infections and number of deaths from HIV have been declining over the past two decades, the lifelong nature of HIV infection means that it will continue to impose a substantial disease burden on global health for the foreseeable future. Despite the high effectiveness of ART, HIV can and does evolve drug resistance, just as it evolves to evade the immune response: over time, an individual's HIV infection may become drug-resistant, preventing effective control of the infection. Therefore, understanding HIV and the biological processes underlying HIV infection remains an important task that provide helpful insights in developing more effective therapies, and perhaps towards a practical cure.

2.2 Basic in vivo mathematical models of HIV

The interaction between HIV and the host's immune system has been the subject of mathematical modeling efforts dating back to at least the early 1990s (12). A very basic model for HIV infection can be described by the following set of ordinary differential equations (ODEs) using the law of mass action:

$$\begin{aligned} \dot{X} &= \lambda - dX - \beta XY, \\ \dot{Y} &= \beta XY - aY - pYZ, \\ \dot{Z} &= cYZ - bZ. \end{aligned} \tag{2.1}$$

The uninfected and infected CD4+ cell populations are denoted by X and Y, respectively. The CTL population, whose growth is stimulated in response to infected cells and which also preys on the infected cells, is denoted by Z. The law of mass action essentially states that the rate of a chemical reaction is directly proportional to the product of the concentration of the reactant species. Treating each interaction between the different populations of cells as a "chemical" reaction, we can derive all the terms in the ODE model.

The dynamics of this model are governed by a number of constant parameters:

- λ, the production rate for uninfected cells.
- d, the natural death rate for uninfected cells.
- β, the infection rate for uninfected cells upon contact with infected cells.
- a, the death rate of infected cells.
- p, the rate at which infected cells are killed by CTLs upon contact.
- c, the CTL population expansion rate upon antigenic stimulation by infected cells.

- b, the natural death rate of CTLs.

These values of these parameters will be discussed in Chapter 3 when the two-compartment model is introduced.

Note that the model assumes the virion population (i.e., extracellular HIV virions) is in a quasi-steady state with the infected cells, and is therefore proportional to the number of infected cells. It is an extension of the well-established theoretical framework for describing the dynamics of virus infections mathematically (13; 14; 15). It also assumes that the primary driver of HIV infection in this model is direct contact between cells (cell-to-cell spread) and does not directly include cell-free spread by free virions, Direct cell-to-cell spread has been suggested to be the primary method by which HIV spreads in lymphoid tissues since CD4+ T-cells are densely packed there and interact with each other frequently, hence this is a reasonable assumption for the models detailed in this dissertation (16; 17).

The presence of the cYZ term in the ODE for the CTL population ($\dot{Z}$) results in a very aggressive expansion of the CTL response in reaction to any infection. It also simplifies the algebra for stability analyses. However, it also implies that if the CTL population reaches zero for any reason, the CTL population will never appear again. This is not consistent with our understanding of human immunity, for this would imply that the human body would never be able to mount an initial response to an infection since the CTL population would be starting from zero. This is particularly important in the context of the emergence of CTL escape mutants, which shall be explored later in Chapter 2.

It is therefore perhaps more appropriate to use the term cY instead of cYZ. The resulting expansion of the immune response is "weaker" than in the model with the cYZ term, but it also allows for the natural emergence of a reactive CTL population in response to an infection. The ODE system is now as follows:

$$\begin{aligned}
\dot{X} &= \lambda - dX - \beta XY, \\
\dot{Y} &= \beta XY - aY - pYZ, \\
\dot{Z} &= cY - bZ.
\end{aligned} \tag{2.2}$$

By setting $\dot{X} = \dot{Y} = \dot{Z} = 0$, one can solve for the equilibria of the ODE system. For this model, there are two equilibria that correspond to physically feasible outcomes of HIV infection (the third has negative populations, and is thus biologically unrealistic):

- One where the infection dies out, leaving only healthy uninfected CD4+ cells (extinction):

  $$X = \frac{\lambda}{d},\ Y = Z = 0.$$

- Another where the infection is able to sustain itself, and all three populations X, Y, and Z are non-zero (establishment):

  $$X = X^*,\ Y = \frac{b(\beta X^* - a)}{cp},\ Z = \frac{(\beta X^* - a)}{p},\ \text{where}$$
  $$X^* = \frac{-(ab\beta + cdp) + \sqrt{(ab\beta + cdp)^2 - 4(ab\beta cdp - b\beta^2 c\lambda p)}}{2b\beta p.}$$

To determine the circumstances under which either equilibrium is locally stable (i.e., the system will evolve towards given a nearby set of initial conditions), one must find the eigenvalues of the Jacobian of the ODE system:

$$J = \begin{pmatrix} \frac{\partial \dot{X}}{\partial X} & \frac{\partial \dot{X}}{\partial Y} & \frac{\partial \dot{X}}{\partial z} \\ \frac{\partial \dot{Y}}{\partial X} & \frac{\partial \dot{Y}}{\partial Y} & \frac{\partial \dot{Y}}{\partial z} \\ \frac{\partial \dot{Z}}{\partial X} & \frac{\partial \dot{Z}}{\partial Y} & \frac{\partial \dot{Z}}{\partial z} \end{pmatrix} = \begin{pmatrix} -\beta Y - d & -\beta X & 0 \\ \beta Y & \beta - pZ - aX & -pY \\ 0 & c & b \end{pmatrix}. \tag{2.3}$$

In order for an equilibrium to be asymptotically stable, the real parts of the eigenvalues of the Jacobian corresponding to that equilibrium must all be negative. The use of a cY instead of cYZ term significantly complicates the algebra and results in some rather long and messy equations for the eigenvalues. Using the Maple 2022 algebraic solver to solve for the eigenvalues of both equilibria and imposing the requirement that the real parts of the eigenvalues are all negative gives the following results:

- The extinction equilibrium is stable when $R_0 = \beta\lambda/ad < 1$.
- The establishment equilibrium is stable when $R_0 > 1$.

R_0 is known as the *basic reproductive ratio* of the virus. Experimental evidence indicates that the median basic reproductive ratio for HIV is approximately $R_0 = 8.0$, which can help inform our parameter choices (18; 19; 25).

HIV-infected cells are assumed to have an average life-span of around 2.2 days, based on experimental observations, which is equivalent to $a = 0.45$ (19). There is a large measured range for the lifespan of uninfected activated CD4+ cells, which can be infected by HIV, ranging from as little as six weeks (42 days) to 164 days (20; 21). For this work, $d = 0.01$ was chosen, which corresponds to a lifespan of 100 days, well within the range of measured values.

The median naive CD4+ cell production rate has been measured to be about 8×10^7 cells per day (22). There are approximately 800 lymph nodes in the human body, so the average number of CD4+ cells entering each lymph node can be conservatively estimated to be 10^5 cells per day (23). HIV preferentially infects activated CD4+ T-cells, and the median CD4+ cell activation fraction has been estimated to be approximately 0.005 per day during chronic HIV infection (24). This means that during chronic HIV infection, we can plausibly estimate that roughly 500 uninfected activated CD4+ cells will be generated each day in a

lymph node, corresponding to $\lambda = 500$.

The parameter β has not been experimentally measured. However, since the median basic reproductive ratio for HIV is approximately 8.0 and we have estimates for λ, a, and d, β can also be estimated using the basic reproductive ratio formula $R_0 = \beta\lambda/ad$. Throughout this paper, we therefore use the values $\lambda = 500$, $\beta = 0.00007$, $a = 0.45$, and $d = 0.01$, resulting in $R_0 = 7.78$, unless otherwise specified.

The infection equilibrium (i.e., non-zero X, Y, Z equilibrium) of the basic in vivo HIV model (2.1) has been shown by Korobeinikov to be globally stable if $R_0 > 1$ (26). Using the same methods, it is straightforward to show that the infection/establishment equilibrium in model (2.2) is also globally stable if $R_0 > 1$ using a Lyapunov function of the form:

$$V = (X - X^* \ln X) + A(Y - Y^* \ln Y) + B(Z - Z^* \ln Z)$$

where A and B are constants and X^*, Y^*, Z^* are the equilibrium populations, with the same techniques used by Korobeinikov.

2.3 Secondary lymphoid tissues and HIV

As noted previously, the majority of the HIV-infected cells and HIV replication (5—10-fold difference compared to peripheral blood levels) can be found in the secondary lymphoid tissues such as lymph nodes and the spleen (27). This means that a proper understanding of HIV infection, particularly during the asymptomatic "latent" phase, must take aspects of the lymphoid tissue environment into account, which is quite different from the peripheral blood environment.

Secondary lymphoid tissues are a critical part of the human immune system and primarily

perform two major functions:

- Filtration of extracellular fluids such as lymph, blood, and interstitial fluid from foreign particles.
- Housing lymphocytes produced in the primary lymphoid tissues (e.g., the thymus) and providing an environment where they can react with foreign antigens to initiate the adaptive immune response.

In light of these functions, secondary lymphoid tissues, unlike peripheral blood, are compartmentalised environments, as illustrated in Fig. 2.3 (28). For the purposes of this dissertation, we divide the lymphoid tissues into two compartments: the B-cell follicles and the extrafollicular tissues.

B-cell follicles are primarily inhabited by B-cells, follicular helper CD4+ T-cells, and follicular dendritic cells (FDCs) (29). Under normal circumstances, FDCs play a critical role as antigen-presenting cells in the adaptive immune response as naive B and T-cells come into contact with the FDCs and become activated. They are also responsible for maintaining the follicular architecture of the lymphoid follicles. B-cells that demonstrate the highest affinity with the antigens presented by the FDCs do not undergo apoptosis (programmed cell death) and instead proliferate, assembling into germinal centers (30). Follicular helper T-cells assist in this process by providing co-stimulation to the B-cells and producing cytokines (31). The activated B-cells then differentiate into antibody-producing plasma cells and long-lived memory cells.

During HIV infection, large amounts of HIV virions (estimated $10^{10}--10^{11}$ virions) can bind to the FDCs. In vitro experiments have found that these FDC-bound virions can remain infectious for at least 25 days and as long as 9 months in this state (32). Even though the FDCs themselves are not productively infected by HIV, the FDC-bound virions are potently

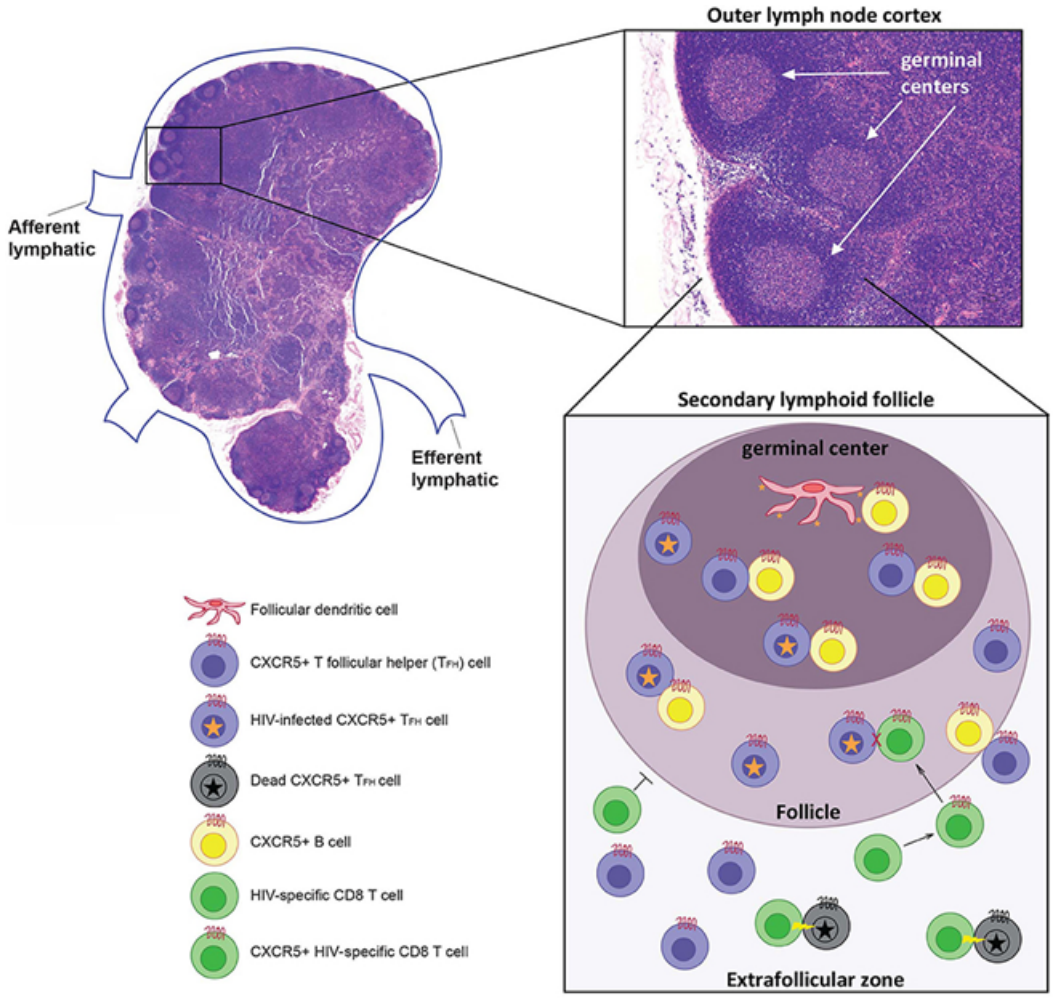

Figure 2.3: Illustration of the structure of a lymph node. Follicles are located in the outer lymph node cortex and primarily house B-cells. When activated by the presence of foreign antigens, the follicles will form germinal centers. Follicles are semi-immune privileged, where CTL activity is inhibited. (Beck et al. (2019) (28))

infectious to the follicular helper T-cells often found in close proximity to the FDCs, even in the presence of large quantities of neutralising antibodies (33; 34; 35). It has therefore been suggested that FDCs play a key role as a long-term reservoir for HIV, allowing it to persist in spite of ART or the immune response. B-cells cannot be infected by HIV since they do not express the CD4 receptor required for HIV to infect.

It is generally thought that CD8+ CTLs are essential for controlling HIV replication, as evidenced by the correlation between the decline in viremia during HIV infection with the appearance of HIV-specific CTLs and CTL depletion experiments using the SIV model (33; 36). While CTLs are present in the secondary lymphoid tissues, they are not commonly found in the B-cell follicles and mostly remain in the extrafollicular tissues. During the acute infection stage, HIV-infected cell concentrations were found to be similar in both the follicular and extrafollicular tissues, whereas in the chronic stage following the appearance of HIV-specific CTLs, the concentration in the extrafollicular tissue is markedly lower. (3) It has also been observed that the concentration of HIV-specific CTLs is much lower in the follicular tissue (40-fold reduction compared to extrafollicular tissue). (37) The exact mechanisms behind the poor infiltration and activity of CTLs in the follicular lymphoid tissues remain poorly understood, although it has been suspected that this may be because very few HIV-specific CTL exhibit the follicular homing phenotype CXCR5+CCR7- during chronic infection. (29)

The basic HIV mathematical models (2.1) and (2.2) clearly do not incorporate any form of compartmental structure and implicitly assume a homogeneous well-mixed environment. Other mathematical models commonly used in modelling HIV dynamics do not usually incorporate this compartmental structure. (38; 39; 40; 41) This is understandable, as it considerably complicates the mathematical analysis of such models, often making it impossible to obtain closed form solutions for the equilibria or stability conditions, unlike with the simpler models (2.1) and (2.2). The homogeneity assumption may be valid for modeling HIV

dynamics restricted to the peripheral blood, but since the vast majority of HIV replication occurs in the compartmentalised secondary lymphoid tissues, a model that wishes to accurately capture HIV dynamics in the human body as a whole must account for this structure. Incorporating this experimentally observed compartmentalisation into HIV mathematical models can have profound consequences, as will be demonstrated in the following chapters.

Chapter 3

Post-ART HIV decline

In this chapter, a two-compartment deterministic model for HIV infection will be presented and be applied to modeling post-anti-retroviral therapy (ART) HIV clearance. It will be shown that compartmentalisation of the secondary lymphoid tissues may explain the puzzling observation that the rate of post-ART HIV clearance is apparently independent of the presence of the CTL response, a finding that has been used to propose that CTLs do not control HIV viremia via cytotoxic effects despite experimental in vivo and in vitro observations that CTLs are potently cytotoxic against HIV-infected cells.

3.1 Anti-retrovirals

The first effective anti-retroviral drug against HIV, the reverse transcriptase inhibitor azidothymidine also known as zidovudine, was approved by the FDA for treating HIV/AIDS patients in 1987. According to the NIH, there are over 30 types of anti-retrovirals drugs approved by the FDA for HIV, which can be divided into seven classes: (9)

- Nucleoside reverse transcriptase inhibitors
- Non-nucleoside reverse transcriptase inhibitors
- Protease inhibitors
- Fusion inhibitors
- CCR5 antagonists
- Integrase strand transfer inhibitors
- Post-attachment inhibitors

All of these anti-retrovirals function by targeting various steps in HIV's reproductive cycle (see Fig. 2.2 in order to block HIV replication and/or prevent HIV from infecting other uninfected CD4+ cells. They are usually given in combination in order to increase their effectiveness and reduce the chance of HIV developing resistance. In most cases, they are highly effective and capable of suppressing measured blood viral loads to below detectable levels. However, they cannot eliminate already-infected cells or the HIV genomes integrated into their DNA. The elimination of infected cells can only occur via their natural death or via the cytotoxic immune response.

Mathematical models of post-ART in vivo HIV dynamics usually assume a single homogeneous environment in which the dynamics take place (38; 42). There are open questions as to whether ART drugs can penetrate effectively into the lymphoid B-cell follicles or the secondary lymphoid tissues: there is at least one study that reports sub-optimal concentrations of ART that may not fully suppress viral replication in secondary lymphoid tissues (43). Conversely, there is a lack of evidence of ART-resistant mutants arising from secondary lymphoid organs, which would be expected to appear if ART did not fully suppress viral replication in these tissues (44).

3.2 CTLs and post-ART HIV dynamics

As mentioned previously in Chapter 1, there is overwhelming evidence that CD8+ CTLs play a crucial role in controlling HIV infection during the chronic phase. It has always been assumed, as befitting the name "cytotoxic", that CTLs accomplish this through direct cytolytic action, killing the HIV-infected cells. This is supported by numerous in vitro and in vivo studies conducted on both HIV in humans and its relative, SIV, in simians, as summarised in Davenport & Petravic (2010) (45).

However, in 2010, Klatt et al. and Wong et al., using similar methods, published experimental results that challenged this assumption (46; 47). Using the simian-SIV model, comparing CTL-depleted SIV-infected rhesus macaques and control groups of rhesus macaques with functional CTL responses, both Klatt et al. and Wong et al. found that there was no difference in the observed lifespan of HIV-infected cells in both groups. This implies that the CTL response (or lack thereof) did not apparently affect the death rate of SIV-infected cells. Klatt et al. further found that this held true with macaques in both the early and late phases of chronic SIV infection, as illustrated in Fig. 3.1. Asquith et al. also report that CTLs are inefficient at killing infected cells in vivo. (48)

As noted by Davenport & Petravic, this observation has potentially important implications for our understanding of HIV infection and the immune response to it. It is difficult to reconcile this apparent lack of cytotoxic activity from the CTL response with other observed in vitro and in vivo results that imply the opposite. The importance of resolving this issue cannot be understated because most prospective anti-HIV vaccines rely on activating the CTL response against HIV. The work in this chapter proposes that perhaps compartmentalisation can reconcile these apparently contradictory observations of potent cytotoxic anti-HIV CTL activity and lack of CTL impact on HIV-infected cell lifespan. However, to do this, we will need a mathematical model that builds in this compartmentalisation and does not assume

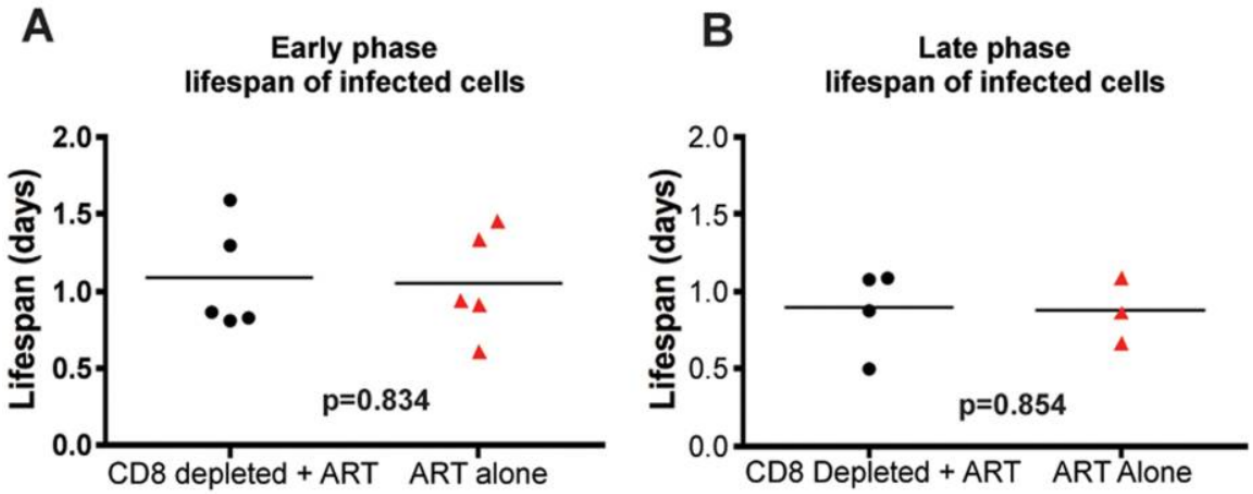

Figure 3.1: Klatt et al.'s results. After ART, there is no significant difference between the lifespan of SIV-infected cells from CD8 (CTL)-depleted and non-depleted macaques, implying the CTLs are not directly killing the infected cells. This occurs in both the early and late chronic phases of SIV infection (Klatt et al. (2010) (46))

a homogeneous medium like the basic HIV models (2.1) and (2.2).

3.3 Two-compartment deterministic model of HIV infection

Consider a two-compartment mathematical model for HIV infection in lymphoid tissue. The lymphoid tissue can be divided into the follicular (F) and extrafollicular (EF) compartments, where HIV can replicate in both. The number of uninfected and infected CD4+ cells in the follicular compartment are denoted by X_f and Y_f, respectively. Similarly, the corresponding populations in the extrafollicular compartment are denoted by X_e and Y_e, respectively. CTLs primarily populate the extrafollicular compartment, denoted by Z_e. CTLs may also enter the follicular compartment, with the population there denoted by Z_f. The average time evolution of the populations in this model can be described by the following set of ODEs using the law of mass action:

$$
\begin{aligned}
\dot{X_e} &= \lambda - dX_e - \beta X_e Y_e, \\
\dot{Y_e} &= \beta X_e Y_e - aY_e - pY_e Z_e - \eta(Y_e - Y_f), \\
\dot{X_f} &= \lambda - dX_f - \beta X_f Y_f, \\
\dot{Y_f} &= \beta X_f Y_f - aY_f - pY_f Z_f - \eta(Y_f - Y_e), \\
\dot{Z_e} &= cY_e - bZ_e - gZ_e + hZ_f, \\
\dot{Z_f} &= gZ_e - bZ_f - hZ_f.
\end{aligned}
\tag{3.1}
$$

The parameters are as follows:

- λ is the production rate for uninfected cells, d is the natural death rate for uninfected cells,
- β is the infection rate (infectivity) for infected cells upon contact with uninfected cells.
- η is the migration rate of infected cells between the compartments.
- a is the death rate of infected cells.
- p is the rate at which infected cells are killed by CTLs upon contact.
- c is the CTL population expansion rate upon antigenic stimulation by infected cells.
- b is the natural death rate of CTLs.
- g is the rate at which CTLs infiltrate into the follicular compartment.
- h is the rate at which CTLs migrate back into the extrafollicular compartment

Note that CTL stimulation is assumed to only occur in the extrafollicular compartment. The follicular tissue of secondary lymphoid tissue is a relatively immune privileged zone where

B-cells reside, where an unchecked CTL response might result in excessive collateral damage. CTLs generally do not enter these follicles unless they express CXCR5 and are less effective at killing infected CD4+ cells than those in the extrafollicular (EF) compartment (29; 28).

This model has previously been examined in Wodarz et al. (2018) (49). It is worth examining some of the basic properties of this model before applying it to modeling post-ART HIV decline. In the limit $\eta \to 0$, it is possible to effectively treat the model as describing two completely separate compartments. In (49), λ and β are defined separately for each compartment (λ_e, λ_f and β_e, β_f). We can define the basic reproductive ratio of HIV in each compartment, given by $R_{0e} = \lambda_e \beta_e / ad$ and $R_{0f} = \lambda_f \beta_f / ad$. Naturally, if both R_{0e} and $R_{0f} > 1$, then HIV will establish itself in both compartments. Without any CTL response ($Z_e = Z_f = 0$), then the equilibrium will be as follows:

$$X_e^* = \frac{a}{\beta_e};\ Y_e^* = \frac{\lambda_e}{a} - \frac{d}{\beta_e};\ X_f^* = \frac{a}{\beta_f};\ Y_f^* = \frac{\lambda_f}{a} - \frac{d}{\beta_f}$$

According to Wodarz et al., it can be shown using the Jacobian of the ODE system (3.1) that if $\eta > 0$, then the infection will be established in both compartments if the following condition is met:

$$\frac{(\beta_f \lambda_f - ad)(\beta_e \lambda_e - ad)}{d\eta(\beta_f \lambda_f + \beta_e \lambda_e - 2ad)} > 1.$$

The resulting exact infection equilibrium expression is far too complicated to give here, but in the limit $\eta \to 0$, it converges to the aforementioned equilibrium, as expected (49).

The addition of CTLs complicates matters somewhat. The CTL population will expand as long as infected cells are present in the extrafollicular compartment, since that is where CTL stimulation (the term cY_e) occurs. The extent of the CTL expansion depends on the infected cell population size. The system then converges towards a stable equilibrium describing CTL-mediated virus control. The full expression for this equilibrium is too complicated to

provide here, but the equilibrium viral load is inversely proportional to the strength of the CTL response, which in this model is determined by the CTL expansion rate/responsiveness (c), and the CTL-mediated killing rate (p). This is similar to the behaviour found in other HIV models with a CTL response (50).

For simplicity, we may assume that the production rate of uninfected cells λ and the infectivity of HIV β are the same in both compartments. They need not necessarily be the same, but there is no evidence that these two parameters differ inside and outside the follicular zone of a lymph node. In order to achieve a scenario where most of the CTLs are in the extrafollicular compartment, as experimentally observed by Connick et al. (3), this requires $g \gg h$.

As noted previously, this two-compartment model has significantly greater complexity, both in the difficulty of solving and mathematically analysing the ODE system and in the resulting trajectories of the populations, compared to the simpler model (2.2). However, as we shall see, it can help explain the apparently lack of influence of CTLs on the post-ART decline rate of HIV/SIV-infected cells, as well as other phenomena to be described in the coming chapters.

3.4 Model application

To model the post-ART decline scenario using (3.1), we must first set an initial population for what is essentially an initial value problem (IVP). This can be done by setting all the left-hand-side terms of (3.1) equal to zero and solving for the populations, and also requiring all the populations to be non-zero. This represents a starting point where chronic infection is established.

The parameter values chosen for this part of the work, except where otherwise noted, are

given in Table 3.1. The reasoning behind the values chosen for λ, β, a, and d was covered in Chapter 2. There is a large amount of uncertainty in the killing rate per CTL-infected cell contact p for HIV/SIV: it ranges from as high as 1.21 to as low as 0.02 (48; 51). The CTL death/response contraction rate b has been estimated to be between 1 and 2 (52). The parameters c, η, g, and h are less well-estimated from observations. Throughout this work we use a range of biologically plausible values for these parameters based on the work of Wodarz et al., with the aim of simulating the segregation and uneven CTL and infected cell populations seen by Connick et al. in lymph nodes (3; 49). We choose g and η values much smaller than h, because if they are of similar scale, then there will be roughly equal rates of migration between the compartments, which will result in more evenly distributed populations, which are not what is observed in the B-cell follicles of lymph nodes and their surroundings.

Parameter table (post-ART model)		
Parameter	Value	Reference
Uninfected cell birth rate, λ	500	(22; 23; 18).
Uninfected cell death rate, d	0.01	(20; 21).
Infected cell death rate, a	0.45	(19).
Contact infection rate, β	7×10^{-5}	From $R_0 = \beta\lambda/ad \approx 8$ (18; 19; 25).
CTL killing rate, p	0.05	(48; 51).
CTL death rate, b	1	(52).
CTL expansion rate, c	0.1	(49).
Infected cell migration rate, η	0.0001	(49).
CTL migration rate (EF to F), g	0.0001	(49).
CTL migration rate (F to EF), h	1	(49).

Table 3.1: Table of parameters for post-ART HIV decline model.

Once we have the initial populations, we can then evolve them using the ODE system. There is no known analytical solution for this IVP, but it is simple enough to solve them numerically using common Runge—Kutta solvers, such as those available in MATLAB or Python's NumPy package. Since we want to model a post-ART scenario, we set $\beta = 0$ for the time evolution because ART halts HIV replication and continued infection of uninfected cells: there are no new infected cells being added to the Y_e or Y_f populations, and they will

decline over time.

For the purposes of this computational experiment, we can "deplete" the CTL response by simply setting $p = 0$, which "turns off" the CTL killing action, mimicking a CTL depletion scenario.

3.5 Results & analysis

Figure 3.2 illustrates the main results of the simulations for the two-compartment model. In Case A, it is clear that the infected cells in the extrafollicular compartment are affected by the presence of the CTL response. This is why the initial decline is significantly faster with CTLs than with the CTLs depleted. The CTL response also has the effect of reducing the initial equilibrium population in the extrafollicular compartment.

In Case B, since the CTLs very rarely infiltrate into the follicular compartment, the presence or depletion of CTLs throughout the body has a negligible effect on both the starting equilibrium population and the post-ART decline rate of infected cells in that compartment.

The decline rate of the extrafollicular infected cells in the non-depleted scenario converges to that of the CTL-depleted scenario. To see why this is the case, consider the rate equations for the Y_e population:

$$\dot{Y_e} = \beta X_e Y_e - aY_e - pY_e Z_e - \eta(Y_e - Y_f)$$

Since there are virtually no CTLs in the follicular compartment, i.e., $Z_f \to 0$, $\beta = 0$, and the very low rate of migration between the two compartments can be neglected, we can

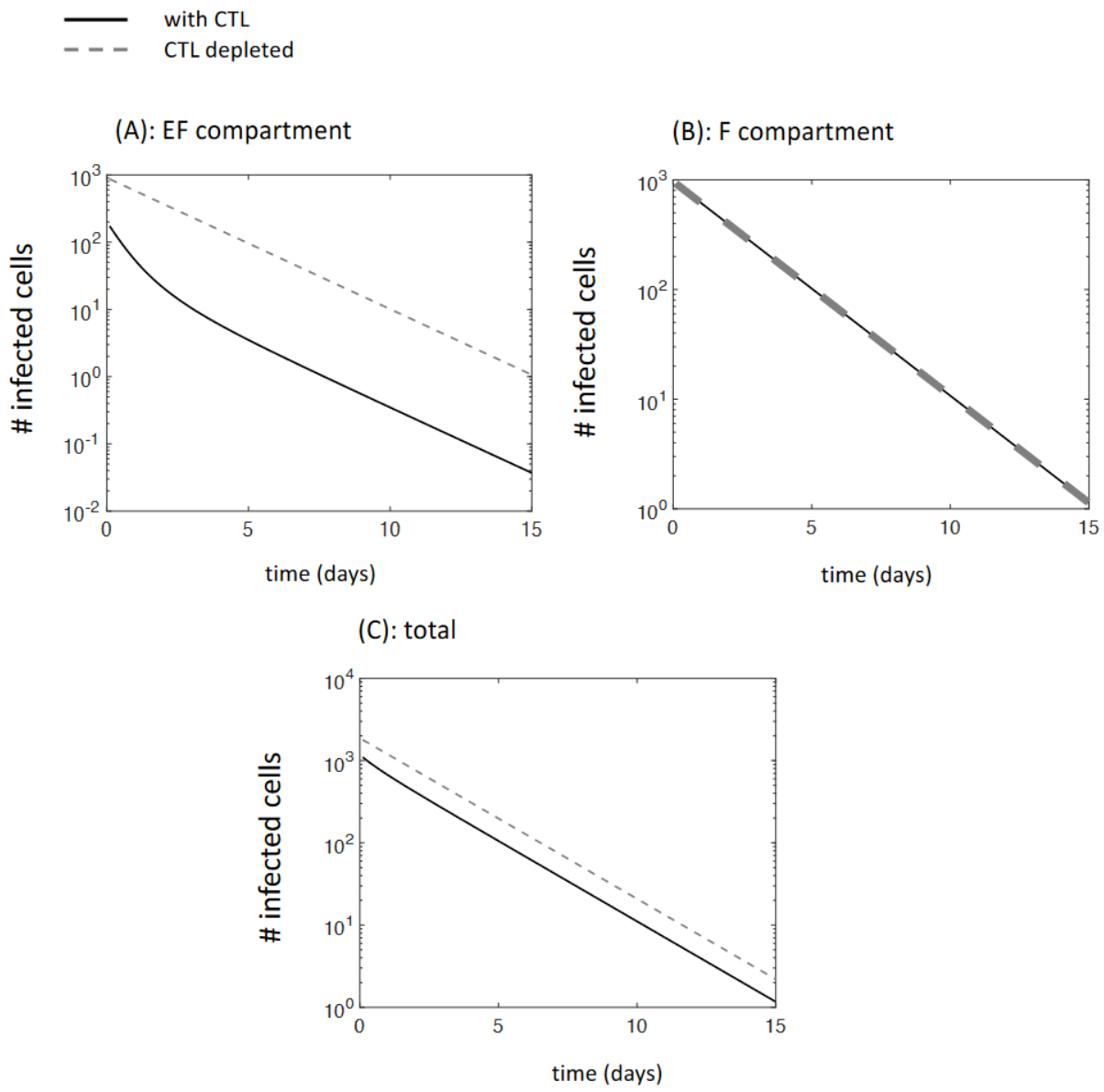

Figure 3.2: Simulations of ODE model (3.1) during ART ($\beta = 0$), in the presence (solid line) and absence (dashed line) of the CTL response. (A) Dynamics in the extrafollicular (EF) compartment. (B) Dynamics in the follicular (F) compartment. (C) Total dynamics, where populations are summed across both compartments.

approximate the rate equation with:

$$\dot{Y_e} \approx -aY_e - pY_eZ_e,$$

while the extrafollicular CTL population can be approximated with

$$\dot{Z_e} \approx cY_e - bZ_e,$$

neglecting the very small amount of CTL migration between the two compartments. In the CTL-depleted scenario, $p = 0$, therefore

$$\dot{Y_e} \approx -aY_e.$$

Since the CTL population Z_e and infected cell population Y_e is high at first, the term pY_eZ_e will dominate at first, while the CTL population is maintained, since it is directly stimulated by the presence of infected cells (term cY_e). However, because of the ART, there is no replenishment of the infected cells, and as their numbers decline, so do the CTL numbers. Because both Y_e and Z_e are both declining, the pY_eZ_e term vanishes faster than aY_e, and eventually we are left with $\dot{Y_e} \approx -aY_e$, i.e., the same rate equation as the CTL-depleted scenario.

In Case C, by combining the total viral load ($Y = Y_e + Y_f$) in both compartments, we can see that the decline rate of the total viral load is virtually the same for the CTL-depleted and non-depleted scenarios, based on the slope of the graphs. Why is this the case? It is because of the uneven CTL distribution in the two-compartment model with $p \neq 0$; this results in the follicular infected cell population being substantially larger than the extrafollicular population, since they are not being depleted by the CTL response. The decline rate of the follicular infected cells is also lower than that of the extrafollicular cells, which therefore means that it is the dynamics in the follicular compartment that dominates, regardless of

the CTL response or lack thereof.

Viral load in the peripheral blood is a measure of the total number of infected cells, and thus its decline would reflect that of the total infected cell decline rate across both compartments in (C). Thus, the two-compartment model can account for the constancy of the viral decline slope irrespective of the strength of the CTL response, even though it assumes that the CTLs themselves can be highly cytotoxic to the HIV-infected cells.

The single-compartment model (2.2), on the other hand, has different behaviour altogether. In order to ensure the starting populations and R_0 of the virus are the same as those of the two-compartment model, the birth rate of uninfected cells λ is set to twice that of the two-compartment model, i.e., $\lambda = 1000$ and the infectivity of the virus is reduced by half, i.e., $\beta = 0.000035$ before it is set to 0 for the simulations. The simulations can be seen in Fig. 3.3.

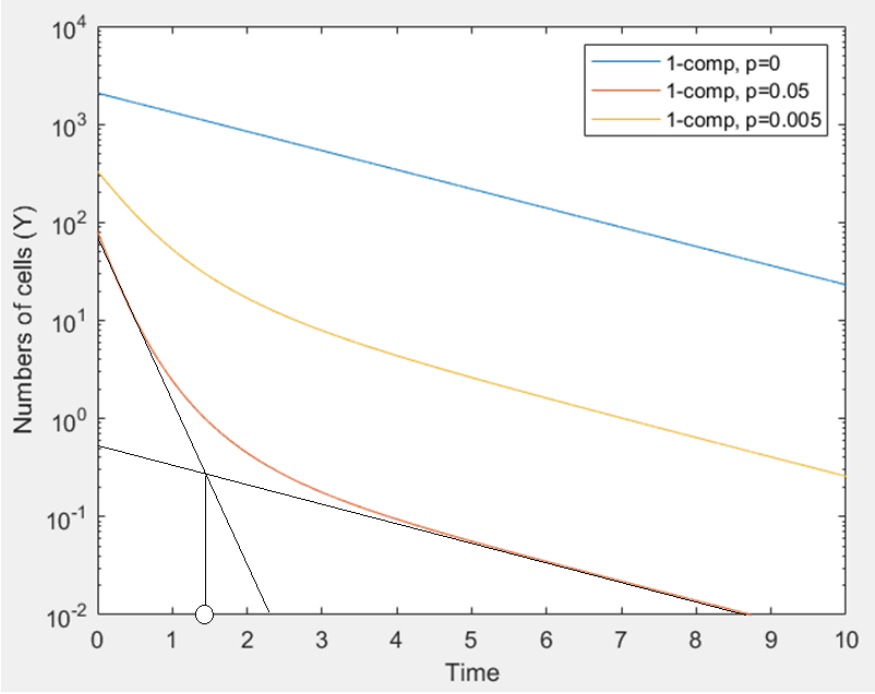

Figure 3.3: Simulations of ODE model (2.2) during ART ($\beta = 0$), for various values of the CTL killing rate p. If the CTL killing is turned off ($p = 0$) then the decline has a constant rate. If $p \neq 0$, then the initial decline rate is faster than at later times. The white circle marks the point at which the slopes change.

The initial decline rate is affected by the CTL killing rate, similar to what occurs in the extrafollicular compartment of the two-compartment model (see Fig. 3.2 (A)). Notably, there is a point at which the decline rate for the total population of infected cells changes from being dominated by the CTL killing action to being dominated by the natural infected cell death rate as the infected cell and CTL populations decline over time, marked by the white circle. Before this point, the behaviour is dominated by the CTL killing action; after it, the natural death rate is more dominant because of the low CTL population. This point does not exist in the two-compartment model's total viral load (see Fig. 3.2 (C)) because the decline there is completely dominated by the much larger follicular compartment, where CTL action is minimal. This provides a potential way of distinguishing between the single and two-compartment models.

It is important to note at this point that these models only take into account lytic CTL-mediated activity and ignores non-lytic suppression of viral replication by the CTL response. The reason is that we would like to investigate the dynamics under lytic activity, for which it has been more difficult to explain the evolutionary dynamics of the virus. There have been models that incorporate two stages for the infected cells in order to reproduce the observed constant decline rate: a cellular eclipse (latent) phase and a virus production phase that is subject to CTL-mediated killing (53). This model shows that such a complication is unnecessary in order to explain the observations, though it does not exclude such a possibility. Additionally, this model does not simulate the longer term virus decline dynamics during ART, which would require a more complex model that tracks infected macrophages and latently infected cells (54). This is beyond the current scope of the analysis and the added complexity is unlikely to change the basic behaviour or conclusion arrived here.

In summary, compartmentalisation in secondary lymphoid tissues and the resulting uneven CTL response can resolve the apparently contradictory observations that CTLs are highly potent against HIV-infected cells, while at the same time CTL depletion does not affect

the decline rate of HIV viral load post-ART. In light of this result, it is suggested that experiments and especially therapies centred around the CTL response should account for this inhomogeneity in the CTL response.

Chapter 4

HIV CTL escape

In this chapter, the two-compartment deterministic model for HIV infection presented in Chapter 3 will be modified and applied to modeling HIV evolution towards escaping the CTL response. It will be shown that compartmentalisation of the secondary lymphoid tissues and the subsequent uneven cross-compartment immune response can offer a safe haven for HIV replication in the face of a robust CTL response. This potentially explains the experimental observation that HIV is relatively slow to evolve an escape towards the CTL response during the chronic phase of infection.

4.1 HIV mutation & genetic diversity

As described in the Background chapter, HIV is a single-stranded RNA virus. In order to turn its single-stranded RNA into DNA, it must under go reverse transcription using an enzyme called reverse transcriptase. Unlike most other DNA polymerases, reverse transcriptase has no "proofreading" mechanism to correct errors (i.e., a wrong base inserted into the genome) occurring during reverse transcription. These errors are mutations in HIV's genome, and

the rate at which these errors are generated is called the mutation rate.

Cell culture studies generally estimate HIV-1's mutation rate to be on the order of 10^{-5} errors per base pair per replication cycle (55). However, at least one in vivo study of HIV genomes in peripheral blood mononuclear cells (which include lymphocytes and monocytes) suggests that the actual mutation rate may be as much as two orders of magnitude higher, at 10^{-3}, with reverse transcriptase contributing only 2% of mutations and the remaining 98% resulting from editing by host cytidine deaminases of the A3 family (56).

As is usually the case for every biological organism, the vast majority of these mutations are either neutral or outright detrimental to HIV's survival. However, occasionally, the mutation may be advantageous to its survival instead. In particular, these mutations can affect the gp120 spike glycoprotein recognised by the immune response, with the point mutations changing the epitope to the point where it cannot be recognised by either the CTL or humoral (antibody) response (58). This process is termed *immune escape*, and it is one of the keys to HIV's survival.

HIV-1 also has an extremely prodigious reproduction rate, estimated at 10^{10} virions/day within a single individual without ART (57). The high reproduction rate and high mutation rate combined lead to exceptional degree of genetic diversity, even compared to other RNA viruses such as influenza. This is illustrated by Fig. 4.1, most notably by comparing the size of the phylogenetic trees for globally circulating influenza strains of 1996 with that for HIV in a *single individual* taken 6 years after infection. Their sizes are broadly comparable, indicating a similar level of genetic diversity (59).

The genetic diversity of HIV strains and HIV's ability to evolve to evade the immune response represent some of the greatest challenges to developing effective treatments and vaccines against HIV. It also underlies the need for total viral replication suppression during ART, as incomplete replication suppression will almost inevitably lead to HIV evolving resistance to

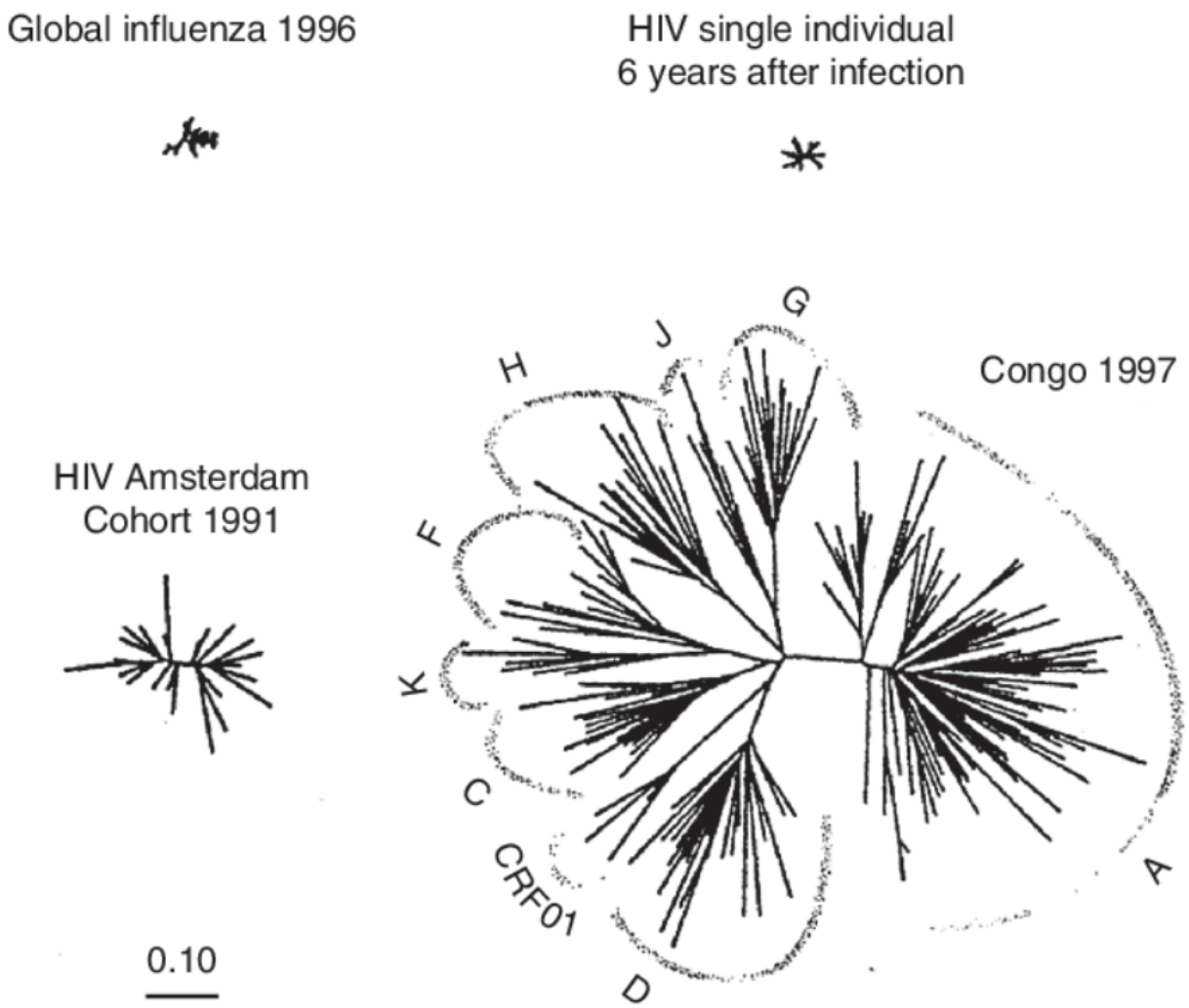

Figure 4.1: Phylogenetic trees of HIV-1 variation and subtypes (clades) of HIV sequences taken from different populations. The length of the spokes from the center of each cluster is in proportion to the degree of variation in the gp41 region of the env gene. The scale bar at the bottom left shows 10% divergence at the amino acid level. Thus, the genetic diversity in a single HIV-infected individual 6 years after infection is broadly equivalent to the global variation in the haemagglutinin gene of seasonal influenza Type A H3N2 in 1996. The variation in the Amsterdam cohort of subtype B infection is correspondingly greater. The longer HIV has been circulating, the greater the variation, hence why the phylogenetic tree from the Democratic Republic of the Congo where HIV-1 has resided longest is immense. (Ndung'u & Weiss (2012) (59))

the ART drug(s) used. This is also the reason why ART uses multiple classes of medications (see Chapter 1) because it is much more improbable for HIV to evolve resistance against different ART drug classes simultaneously.

4.2 HIV's "slow" CTL escape

On a fundamental level, the viral adaptation rate against the immune response is proportional to two factors. One is the strength of the immune response, which for our purposes can be taken to be the CTL response. The stronger the immune response is, the greater the selective pressure on the virus to evolve to escape it.

The other is the viral abundance, i.e., number of infected cells. More infected cells results in greater viral reproduction, and thus a higher rate of mutant production, increasing the likelihood of an escape mutant strain appearing. However, the immune response strength is also inversely proportional to the viral abundance: the greater the CTL response, the more infected cells will be killed, thus suppressing viral reproduction.

Qualitatively then, the relationship between the immune response strength and the viral adaptation rate can be illustrated by Fig. 4.2, from Saad-Roy et al. (2021) (60). There is clearly a "Goldilocks" effect at play here: too much immune pressure results in low viral abundance and a low adaptation rate, while too little immune pressure ends up weakening the selective pressure on the virus and this also results in a low adaptation rate.

Despite its high mutation rate, the time it takes for HIV to escape the immune response by evolving an escape mutation to a targeted epitope is longer than expected. In fact, it has been experimentally observed in HIV-positive patients that it takes an average of over two years for an HLA-restricted HIV epitope (i.e., one that can be targeted by the immune response) even with a CTL response to evolve an escape mutation (61). This is illustrated

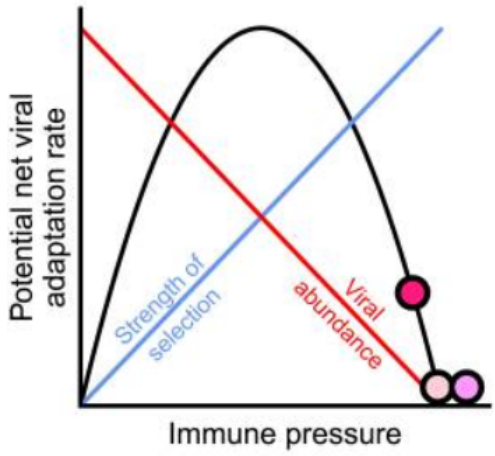

Figure 4.2: Qualitative illustration of the relationship between net viral adaptation rate and immune pressure (black). It can be thought of roughly as the sum between two factors: strength of selection (blue), which is directly proportional to immune pressure, and viral abundance (red), which is inversely proportional to immune pressure. (Saad-Roy et al. (2021) (60))

in Fig. 4.3 taken from (61). As many as 1/3rd of the patients did not drive a CTL escape variant within the first 2 years.

Some explanations have been proposed to explain this curious phenomenon, based on mathematical simulations:

- HIV can also establish latency in infected cells, allowing it to lie dormant and evade the CTL response or ART, which only targets cells where HIV replication is active. Once these pressures subside, the latently infected cells can reactivate, resuming the infection process. (8) Doekes et al. suggest that latently infected CD4+ T-cells can severely delay evolutionary dynamics within a single host, with the size of the latent reservoir and level of homeostatic proliferation of cells within the reservoir having significant effects on the time it takes for escape to evolve. (62)

- Van Deutekom et al. also propose that the breadth of the immune response from the CTLs will affect the rate of immune escape. The broader the immune response to different HIV epitopes, the slower the rate of escape. (53)

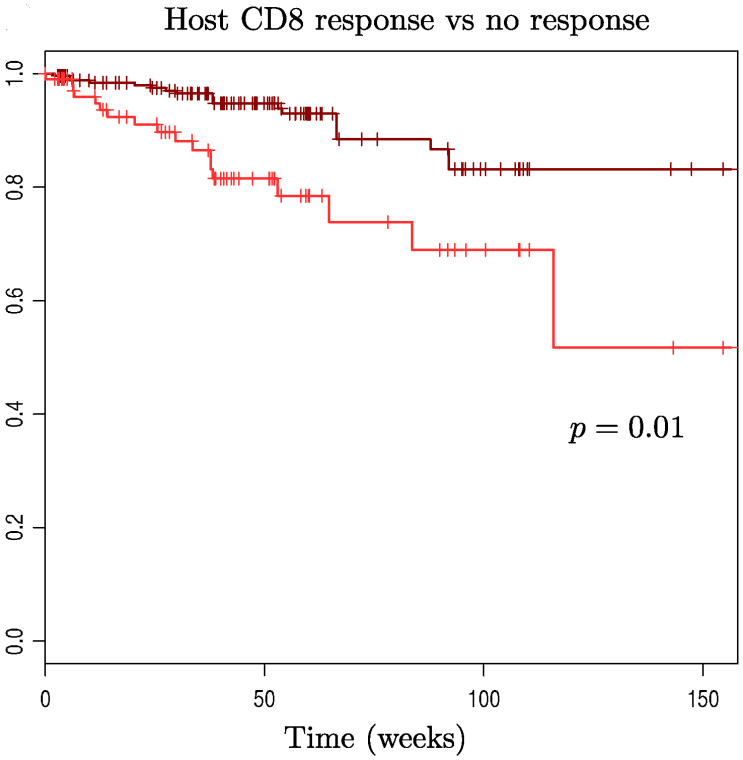

Figure 4.3: Epitopes in HLA-matched hosts are split according to whether they have a measurable CTL (CD8+) response to them (light red) or not (dark red). Escape is significantly faster if the host has a measurable CTL response to that epitope, but even in that case it takes over 2 years for 50% of the epitopes to escape the CTL response. (Roberts et al. (2015) (61))

- Davenport et al. showed that the timing of the immune response as well as the associated fitness costs with evolving an escape response can greatly affect the rate of escape. (63)

Most of the mathematical models used to arrive at these conclusions are single compartment models that do not take into account the existence of the actively replicating follicular reservoirs and the degree of compartmentalization that exists in secondary lymphoid tissue when it comes to the CTL response there. (13; 14; 15; 16) This is a potentially important missing element, especially because these tissues are where most HIV replication occurs.

In Chapter 1, we showed that compartmentalisation and the uneven CTL response can slow down post-ART HIV viral load decline, and it is plausible to think that these may be playing a role in the experimentally observed slow CTL escape rate. Of course, this is not to say that these explanations are wrong or mutually exclusive with the compartmentalisation hypothesis. All of them may play a part in delaying the evolution of CTL escape HIV mutants.

4.3 Two-compartment deterministic model of HIV infection with CTL escape mutation

The single-compartment ODE system (2.2) can be modified to model the emergence of HIV escape mutants as follows:

$$\begin{aligned}
\dot{X} &= \lambda - dX - \beta XY - \beta_1 XY_1, \\
\dot{Y} &= \beta(1-\mu)XY - aY - pYZ, \\
\dot{Y_1} &= \mu\beta XY + \beta_1 XY_1 - aY_1, \\
\dot{Z} &= cY - bZ.
\end{aligned} \tag{4.1}$$

Here, HIV escape mutants are represented by the population Y_1, with the original "wild" type kept as Y. The escape mutants have their own infection rate parameter β_1. It is known that most mutations to the HIV genome lower the virus' reproductive fitness, including those that confer escape from a host's immune response. It is therefore reasonable to expect that $\beta > \beta_1$. Conversely, this model assumes total escape for the mutant strain, thus there is no CTL response against it (i.e., no pY_1Z term). The parameter μ is the mutation rate. For the sake of simplicity, it is assumed that a point mutation gives rise to viral escape. Mutation only occurs during viral replication, thus the $\mu\beta XY$ term represents mutant production from the reproduction of the wild Y type.

By again setting $\dot{X} = \dot{Y} = \dot{Y_1} = \dot{Z} = 0$, one can solve for the equilibria of the ODE system as usual. Two of these have relatively simple forms:

- One with only healthy uninfected CD4+ cells: $X = \lambda/d$, $Y = Y_1 = Z = 0$ (extinction).
- One where the mutant takes over: $X = a/\beta_1$, $Y_1 = (\beta_1\lambda - ad)/a\beta_1$ and $Y = Z = 0$ (fixation).

The same stability analysis as for the equilibria of (2.2) was done with the associated Jacobian:

$$\begin{aligned} J &= \begin{pmatrix} \frac{\partial \dot{X}}{\partial X} & \frac{\partial \dot{X}}{\partial Y} & \frac{\partial \dot{X}}{\partial Y_1} & \frac{\partial \dot{X}}{\partial z} \\ \frac{\partial \dot{Y}}{\partial X} & \frac{\partial \dot{Y}}{\partial Y} & \frac{\partial \dot{Y}}{\partial Y_1} & \frac{\partial \dot{Y}}{\partial z} \\ \frac{\partial \dot{Y_1}}{\partial X} & \frac{\partial \dot{Y_1}}{\partial Y} & \frac{\partial \dot{Y_1}}{\partial Y_1} & \frac{\partial \dot{Y_1}}{\partial z} \\ \frac{\partial \dot{Z}}{\partial X} & \frac{\partial \dot{Z}}{\partial Y} & \frac{\partial \dot{Z}}{\partial Y_1} & \frac{\partial \dot{Z}}{\partial z} \end{pmatrix} \\ &= \begin{pmatrix} -\beta_1 Y_1 - \beta Y - d & -\beta X & -\beta_1 X & 0 \\ \beta(1-\mu)Y & \beta(1-\mu)X - a - pZ & 0 & -pY \\ \mu\beta Y + \beta_1 Y_1 & \mu\beta X & \beta_1 X - a & 0 \\ 0 & c & 0 & -b \end{pmatrix}. \end{aligned} \tag{4.2}$$

Once again solving for the eigenvalues of the Jacobian evaluated at each equilibrium, using the Maple 2022 algebraic solver gives the following conditions:

- the extinction equilibrium is stable when $R_{0,1} = \beta_1\lambda/ad < 1$ and $\beta\lambda(1-\mu)/ad < 1$,
- the fixation equilibrium is stable when $R_{0,1} = \beta_1\lambda/ad > 1$ and $\beta_1 > \beta(1-\mu)$.

where $R_{0,1}$ is the basic reproductive ratio of the mutant strain.

These conditions are fairly intuitive: the former simply occurs when neither strain is capable of sustaining an infection (for the wild strain, either it also has to compensate for the loss during reproduction due to mutation), and the latter will occur when the escape strain does not lose enough fitness from its mutation to be unable to out-compete the wild strain. There are other equilibria as well that can be obtained by solving a complicated cubic equation; the coexistence equilibrium where both strains persist (i.e., $R_{0,1} > 1$, $\beta\lambda(1-\mu)/ad > 1$, and $\beta_1 < \beta(1-\mu)$) is one of those solutions.

We now turn to the two-compartment model:

$$\begin{aligned}
\dot{X_e} &= \lambda - dX_e - \beta X_e Y_e - \beta_1 X_{1e} Y_{1e}, \\
\dot{Y_e} &= \beta(1-\mu) X_e Y_e - aY_e - pY_e Z_e - \eta(Y_e - Y_f), \\
\dot{X_f} &= \lambda - dX_f - \beta X_f Y_f - \beta_1 X_{1f} Y_{1f}, \\
\dot{Y_f} &= \beta(1-\mu) X_f Y_f - aY_f - pY_f Z_f - \eta(Y_f - Y_e), \\
\dot{Y_{1e}} &= \beta\mu X_e Y_e + \beta_1 X_e Y_{1e} - aY_{1e} - \eta(Y_{1e} - Y_{1f}), \\
\dot{Y_{1f}} &= \beta\mu X_f Y_f + \beta_1 X_f Y_{1f} - aY_{1f} - \eta(Y_{1f} - Y_{1e}), \\
\dot{Z_e} &= cY_e - bZ_e - gZ_e + hZ_f, \\
\dot{Z_f} &= gZ_e - bZ_f - hZ_f.
\end{aligned} \tag{4.3}$$

Built on the model of the previous section, we introduce two new populations: Y_{1e} and Y_{1f}

(cells infected by a mutant strain able to evade the immune response), We also introduced a new parameter associated with these populations: β_1, the infectivity of the mutant strain upon contact with uninfected cells.

Unless otherwise noted, the base parameters used in the compartmentalised escape model are given in Table 4.1 The reasoning behind these parameters (other than μ) was already discussed in Chapters 2 and 3. $\mu = 2 \times 10^{-5}$ was selected based on the experimentally observed HIV mutation rate, which is on the order of 10^{-5} (55). c is allowed to vary for within the range $c = 0.0001$ to $c = 10$ in order to investigate the effect of CTL pressure on the system.

Parameter table (HIV escape model)		
Parameter	Value/Range	Reference
Uninfected cell birth rate, λ	500	(22; 23; 18).
Uninfected cell death rate, d	0.01	(20; 21)
Infected cell death rate, a	0.45	(19)
Contact infection rate, β	7×10^{-5}	$R_0 = \beta\lambda/ad \approx 8$. (18; 19; 25)
Contact infection rate (mutant), β_1	0.99β	Plausible fitness cost.
CTL killing rate, p	0.05	(48; 51)
CTL death rate, b	1	(52)
CTL expansion rate, c	10^{-3}–10	(49)
Infected cell migration rate, η	0.0001	(49)
CTL migration rate (EF to F), g	0.0001	(49)
CTL migration rate (F to EF), h	1	(49)
Mutation rate, μ	2×10^{-5}	(55)

Table 4.1: Table of parameters for HIV escape model.

Assume that the fitness cost of the escape mutation is such that $\beta_1 < \beta(1-\mu)$ and complete mutant fixation does not occur. First consider strong compartmentalization, i.e. a low rate of virus exchange, η, between compartments and a low rate of CTL migration, g, into the follicular compartment (Figure 4.4). This regime is intended to model the compartmentalised lymph node scenario described in (3) and (29). A strong CTL response suppresses the virus in the extrafollicular compartment, and that the escape mutant dominates in the EF compartment, while it remains a minority in the follicles due to the low CTL activity and

hence selection there (Figure 4.4 (i)). This is similar to what happens in the early chronic phase of infection. If the CTL response is weaker than a certain threshold, the escape mutant remains a minority in both compartments (Figure 4.4 (ii)). This may simulate an advanced disease stage where the CTL response is exhausted.

On the other hand, the weak compartmentalization scenario simulates a highly mixed system where both virus-infected cells and CTLs migrate often between compartments (larger values of h and g; see Figure 4.5). This is not what is observed in (3), but serves as a point of comparison. The outcome in both compartments is always identical because the CTLs are more or less equally distributed. If the CTL response is strong (high c), the escape mutant dominates in both compartments (Figure 4.5 (i)). For relatively low values of c, the escape strain represents only a minority in both compartments (Figure 4.5 (ii)).

4.4 Gillespie simulations of the two-compartment HIV CTL escape model

The process of mutation is fundamentally random and probabilistic due to the random nature of genetic mutations due to errors in RNA transcription during the HIV replication process. (64) It is therefore not completely appropriate to model this system using deterministic differential equations and we must transition towards using *stochastic* simulations (53). In particular, for small populations, population fluctuations can sometimes lead to situations where extinction occurs where a deterministic model might predict otherwise. Even with high viral loads (populations), stochastic effects can be important (65).

For this work, we used the Gillespie stochastic simulation algorithm (66). This is a Monte Carlo method that starts by sampling two uniformly distributed random numbers r_1 and r_2 from the interval $[0, 1]$. We can think of the evolving dynamical system from HIV infection

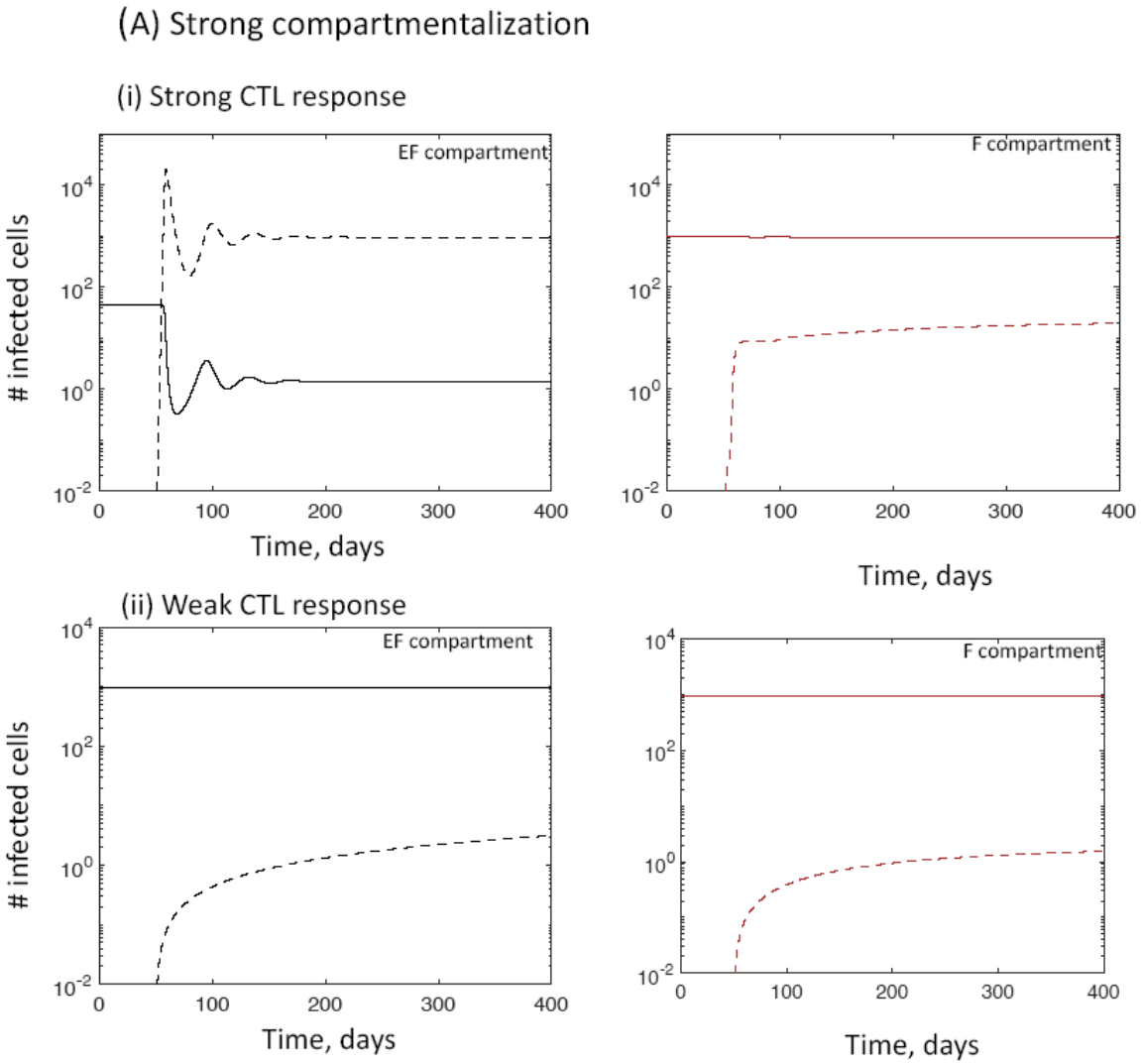

Figure 4.4: Outcomes in ODE model (4.3), including a CTL escape mutant. (A) These plots assume strong compartmentalization, i.e. infected cells move between compartments with a relatively slow rate, and CTL enter the follicular compartment with the slow rate, $\eta = g = 0.0001$. Dynamics are shown for (i) a relatively strong CTL response ($c = 1$) and (ii) for a relatively weak CTL response ($c = 10^{-4}$). Left and right graphs show dynamics in the extrafollicular and follicular compartments, respectively. Solid lines depict the dynamics of the wild-type virus, dashed lines the dynamics of the CTL escape mutant.

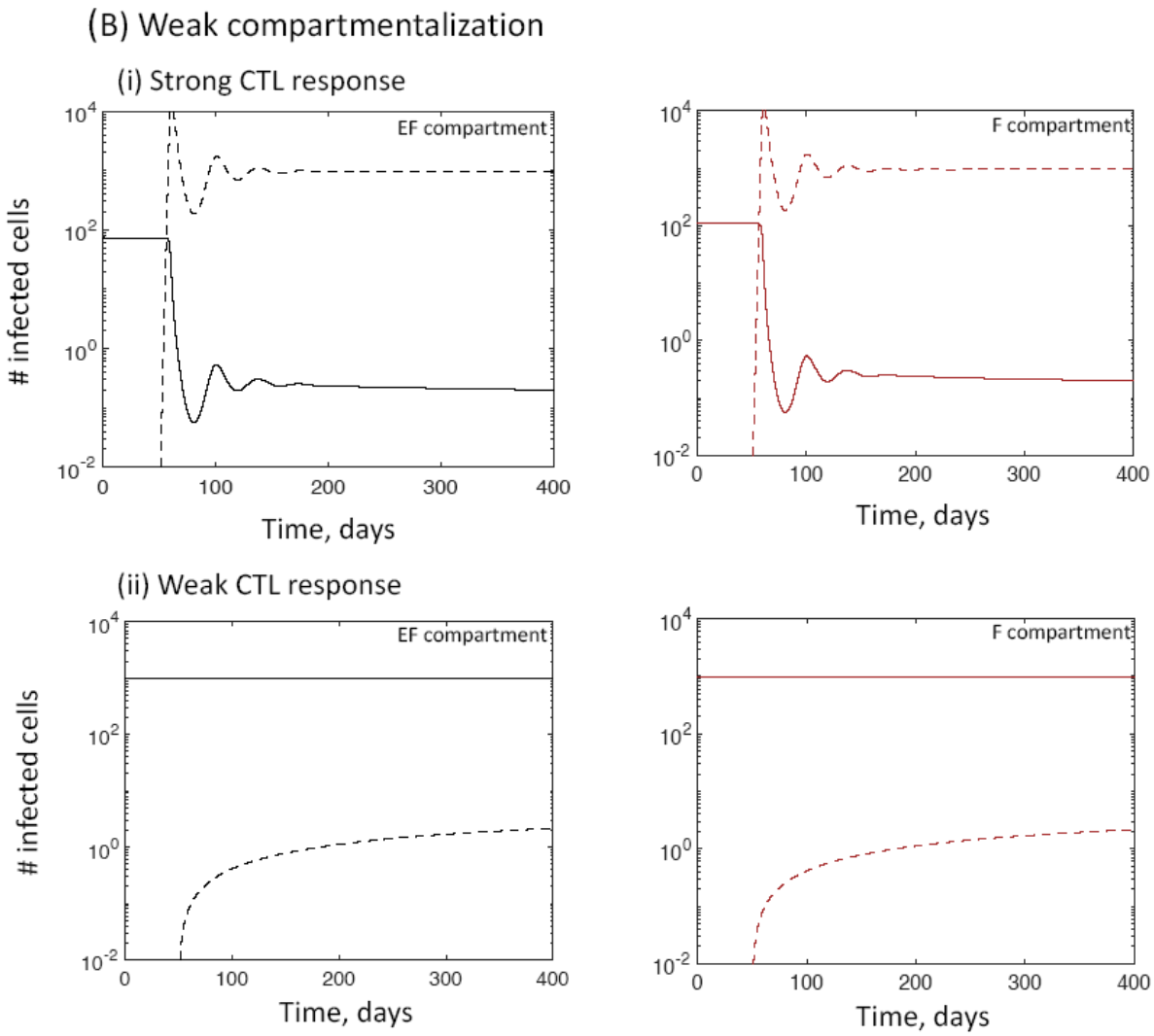

Figure 4.5: Outcomes in ODE model (4.3), including a CTL escape mutant. (B) Same graphs as in Fig. 4.4, but under the assumption that infected cells move with a faster rate between compartments and CTL move to the follicular compartment with a high rate, identical to the rate at which they move from the F to the EF compartment. For (B) $\eta = g = 1$. For strong CTL responses, $c = 1$. For weak CTL response $c = 10^{-4}$.

as a series of events or "chemical reactions" where each event is only dependent on the event that happened immediately before it (i.e., a Markov chain). The first random number is used along with the starting populations (starting from an equilibrium solved using the ODE system (1), i.e., a system where no mutant strains have occurred yet) to compute the time until the next "reaction", τ:

$$\tau = \frac{1}{R_{tot}} \log\left(\frac{1}{r_1}\right), \tag{4.4}$$

where $R_{tot} = \sum_j a_j$ is the total "reaction" rate from summing all the non-duplicated terms in the ODE (3) (e.g., $a_1 = \lambda$, $a_2 = dX_e$, $a_3 = \beta X_e Y_e$, $a_4 = aY_e$, etc.) except for the random mutation terms with μ. These are handled separately.

The second random number r_2 is used to determine what "reaction" takes place after that time by computing the integer n which satisfies the following equation:

$$\sum_{j=1}^{n-1} a_j \leq r_2 R_{tot} \leq \sum_{j=1}^{n} a_n, \tag{4.5}$$

and the populations are adjusted according to the reaction that took place. For example, if $n = 3$, then the reaction that takes place is the one corresponding to $a_3 = \beta X_e Y_e$:

$$X_e + Y_e \rightarrow Y_e + Y_e$$

therefore we would raise the population of Y_e by 1 and lower the population of X_e by 1. However, we must also account for mutation from the original strain (Y_e) to the intermediate escape one (Y_{1e}). To do this, we sample a third random number r_3 from the interval $(0, 1)$.

If $r_3 \leq \mu$, instead of raising the population of Y_e by 1, we instead raise the population of Y_{1e} by 1. Mutation for the other populations involving μ is modeled in a similar way. The reader is advised to refer to Figure 4.6 for a diagram illustrating the various "reactions".

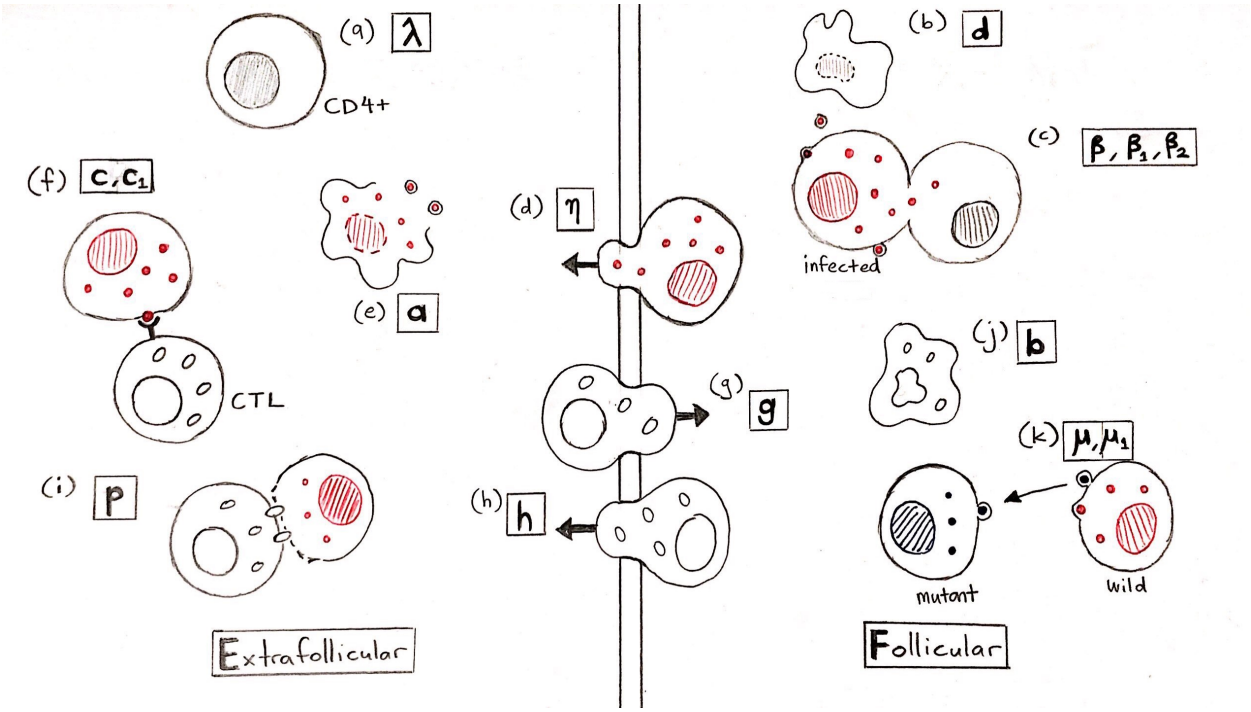

Figure 4.6: Diagram of the various "reactions" in the stochastic model and associated rate constants. The processes are: (a) CD4+ cell birth (λ), (b) uninfected CD4+ cell death ($dX_{e/f}$), (c) HIV infection of uninfected CD4+ cell by contact with infected cell ($\beta X_{e/f} Y_{e/f}$ and $\beta_1 X_{1e/1f} Y_{1e/1f}$), (d) migration of infected cells between the follicular and extrafollicular compartments ($\eta X_{e/f}$ and $\eta X_{1e/1f}$), (e) infected cell death ($aY_{e/f}$ and $aY_{1e/1f}$), (f) activation of CTL response (cY_e), (g) migration of extrafollicular CTLs into the follicular compartment (gZ_e), (h) migration of follicular CTLs out of the follicular compartment (hZ_f), (i) infected cell killed by CTL upon contact ($pY_{e/f} Z_{e/f}$), (j) CTL natural death ($bZ_{e/f}$), and (k) viral mutation ($\mu\beta X_{e/f} Y_{e/f}$)

For each set of parameters, a large number of simulations ($> 1,000,000$) are run for each parameter and the mean takeover time for the escape strain $Y_1 = Y_{1e} + Y_{1f}$ is computed. Takeover time is defined as the time it takes for the population of the complete escape strain Y_2 to reach $Y_1/Y_{tot} = 0.95$, where $Y_{tot} = Y_e + Y_f + Y_{1e} + Y_{1f}$. Each simulation is run until either takeover is achieved or all populations of the virus go extinct, in which case that run is not counted towards the statistics.

Stochastic simulations were run for both models (4.3) and (4.1). For (4.1), $\beta = 0.000035$ and $\lambda = 1000$ were used in order to maintain the same uninfected cell generation rate as the two-compartment model, while also keeping the basic reproduction ratio R_0 identical between both models. The starting populations for all models are determined using the appropriate ODEs by solving for an equilibrium where the infected cell, uninfected cell, and CTL populations are non-zero with mutations turned off ($\mu = 0$). The populations are then evolved using the Gillespie algorithm with $\mu \neq 0$.

Three model versions are compared:

- Model (i) is characterized by strong compartmentalization ($h = g = 0.0001$).
- Model (ii) still has compartments, but populations move between them with relatively high rates ($h = g = 1$).
- Model (iii) is the single-compartment model (4.1).

The value of c on the x-axis corresponds to model (i), and is varied from low to high. For each value of c for model (i), we adjust the corresponding value in model versions (ii) and (iii) such that total viral load is identical across the model versions, eliminating additional effects occurring as a result of variation in the viral load).

In addition to the takeover time, the contribution of the extrafollicular and follicular compartments to mutant evolution is also tracked via the origin of the escape mutants in the computer simulations. When the total mutant infected cell fraction in the extrafollicular compartment reached 95%, we determined in which compartment the largest escape clone originated, and thus recorded the fraction of simulation runs in which the largest escape clone originated in the extrafollicular and follicular compartments, respectively. The results and their analyses are given in the next section.

4.5 Results & analysis

The main results are illustrated in Fig. 4.7. Let us first consider model (i), represented by the purple lines. As is typical for virus dynamics models, total viral load at equilibrium declines with greater CTL responsiveness, c. However, due to the compartmentalization, the decline in the viral load is restricted almost entirely to the extrafollicular (EF) compartment (Fig. 4.7(A)). The follicular (F) compartment is not significantly affected by the greater CTL proliferation, due to the assumed slow rate at which CTLs enter the F compartment.

Fig. 4.7 (B) shows that the average time to mutant invasion has a minimum for an intermediate strength of the CTL response, c. This what one would expect, bearing in mind Fig. 4.2 qualitatively describing net viral adaptation rates from earlier in the chapter. For weak CTL responses, the viral load is high in both compartments and the selection pressure is low. While mutants are generated at a relatively fast rate, their ability to rise at the expense of the wild-type virus is limited because of the low selection pressure. For strong CTL responses, there is high selection pressure in the EF compartment, which facilitates escape mutant invasion. Due to the low viral loads in the EF compartment, however, the probability to generate a mutant is low, which contributes to the increased invasion times.

Mutants are generated more rapidly in the F compartment, where the viral load is higher. However, due to the limited CTL activity in the F compartment, the generated mutants are unlikely to rise to significant levels. They are more likely to go extinct instead, especially because they are assumed to carry an intrinsic fitness cost. For intermediate rates of CTL proliferation, the viral load in the EF compartment is intermediate, providing a higher chance to generate the CTL escape mutant, while the selection pressure still favors the escape mutant to a sufficient extent. This results in the shortest mutant invasion times.

The mutants are overwhelmingly preferentially generated in the EF compartment over a wide range of CTL expansion rates (Fig. 4.7 (C)). Recall that in the F compartment, very

few CTLs are present and the escape mutant is assumed to carry an intrinsic fitness cost. The mutant is thus not likely to emerge in the follicles and move to the EF compartment, given the low inter-compartment migration rate.

For very strong CTL responses, however, escape mutants originate more frequently in the F compartment. In this regime, the CTL response essentially eliminates the virus from the EF compartment, which is only maintained there by influx from the follicles. It is thus more likely that escape mutants are produced in the follicle and subsequently move to the EF compartment, rather than originating in the EF compartment.

Let us now turn out attention to the other models (ii) and (iii). Since these models have the same total viral loads as model (i) by design, this allows us to isolate the effect of compartmentalisation from other potential confounding factors. Starting with model (ii), which still has a compartmental structure and is represented by the green lines, the fast migration rates between compartments renders the system more mixed, resulting in the virus being almost equally abundant in both the F and EF locations (Fig. 4.7 (A), green). Hence, both compartments also contribute equally to escape mutant production (Fig. 4.7 (C), green).

Comparing the average time to escape mutant dominance between models (i) and (ii), different patterns can be observed depending on the strength of the CTL response. For relatively strong CTL responses (c above a threshold), the average time to mutant dominance is significantly longer for the strong compartmentalisation (i) than for weak compartmentalisation (ii) (green vs. purple). In other words, strong compartmentalisation significantly delays the rate at which CTL escape mutants invade in the EF compartment. With strong compartmentalisation, the low selection pressure in the F compartment makes it unlikely for mutants to emerge there and take over the EF compartment; at the same time, the strong CTL-mediated virus control in the EF compartment results in infrequent mutant production there.

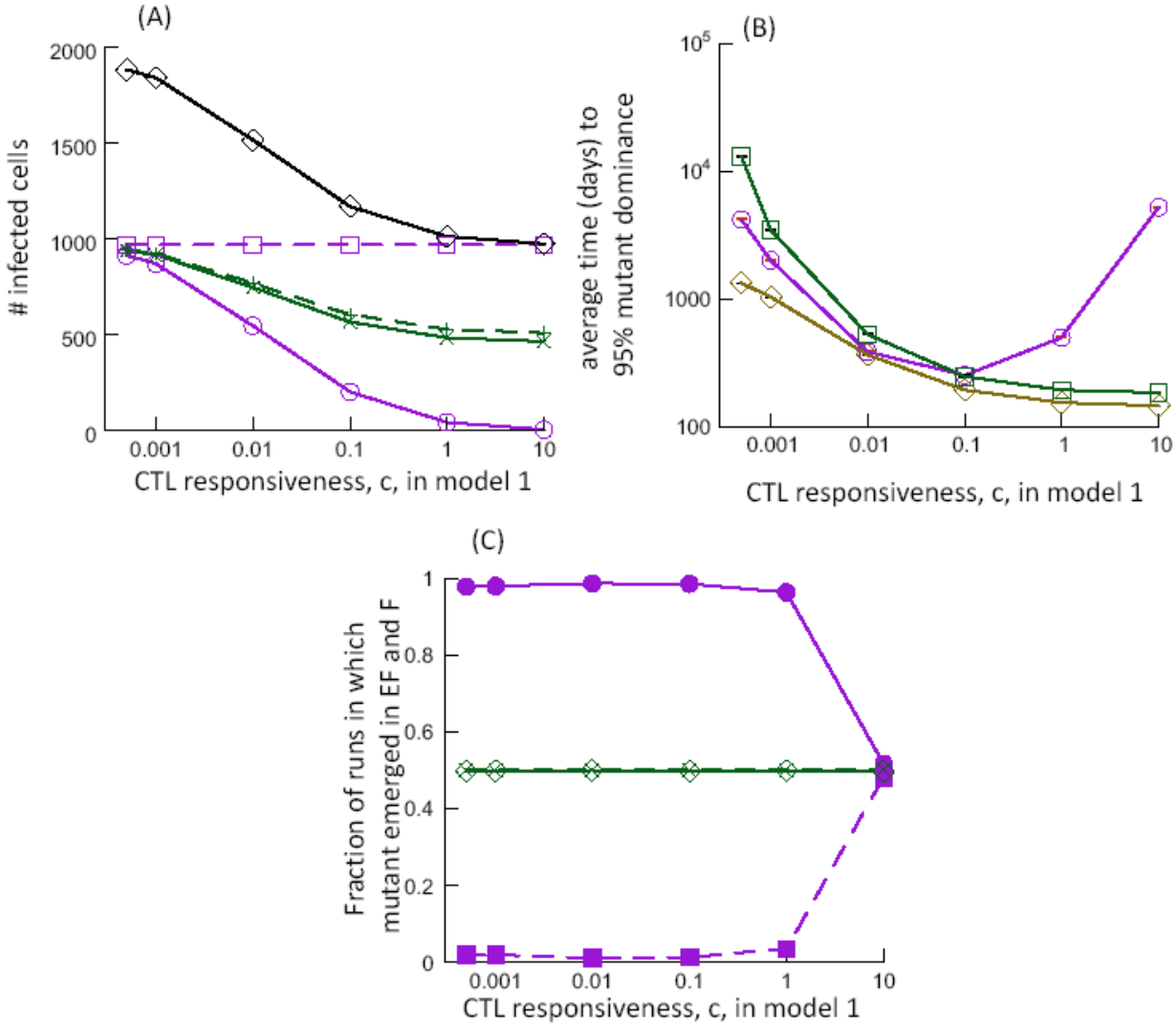

Figure 4.7: Stochastic evolutionary dynamics of CTL escape, as a function of CTL responsiveness, c. Gillespie simulations of ODE model (4.3) were performed. (A) Total wild-type virus load (without mutants) as a function of the parameter $c$in model (i). These are the values predicted by the ODEs and represent the stochastic averages. The black line denotes total virus load, which is kept identical across all three model versions. The purple and green lines show virus load by compartment for models (i) and (ii) respectively. Solid and dashed lines depict the F and EF compartments, respectively. (B) The average time for the CTL escape mutant to reach 95% of the infected cell population in the EF compartment. Purple is model (i), green model (ii), and brown model (iii). Standard errors are shown as error bars but are small and difficult to see. (C) Fraction of simulation runs in which the invading CTL escape mutant was generated in the F (dashed line) and the EF (solid line) compartment. Purple is model (i) and green model (ii). For the compartmental model (i): $\eta = g = 0.0001$. For model (ii), parameters were identical, but with $\eta = g = 1$. For the single compartment model (iii): $\lambda = 1000$; $\beta = 7 \times 10^{-5}$.

In contrast, for weak compartmentalisation (ii), there is significant selection pressure in both compartments, and the viral load in each compartment is intermediate (Fig. 4.7 (A)). This leads to overall faster mutant production, coupled by relatively strong selection. The situation, however, reverses for weak CTL responses (smaller c). Now, the strong compartmentalisation (i) accelerates mutant invasion in the EF compartment, compared to model (ii) (Fig. 4.7 (B)). In this setting, the viral load in the EF compartment is relatively high, even with strong compartmentalisation, due to the weaker CTL response. This results in more frequent mutant production, and concomitant selection of the produced mutants. For weaker compartmentalisation (ii), on the other hand, the CTLs stimulated in the EF compartment can readily move to the F compartment. This lowers the total number of CTLs in the EF compartment, leading to reduced selection pressure and slower mutant invasion.

The single-compartment model (iii), represented by brown lines lacks any compartmental structure and is more typical of previous mathematical models that considered the evolution of immune escape (Fig. 4.7 (B), brown). Escape mutant invasion occurs fastest here (compared to both models (i) and (ii)). In the strongly compartmentalised model (i), the overall viral load is given by the sum of the low number of infected cells in the EF compartment and the large number of infected cells in the F compartment, due to the uneven CTL activity. To achieve a comparable total viral load in the single compartment model (version iii) requires a CTL response of only intermediate strength. As in Fig. 4.2, this results in intermediate virus load in the single compartment, together with significant selection pressure, and this promotes escape mutant invasion.

In summary, for a fixed total viral load, both compartmentalised models (i) and (ii) predict a significantly longer time for escape mutant invasion to complete compared to the single-compartment model (iii). This again highlights the role of compartmentalisation in delaying CTL escape mutant evolution. This can be attributed to the partitioned and uneven CTL population in the compartments, which, even in the face of strongly responsive CTLs that

could apply a lot of selection pressure, allows the follicles to maintain a large reservoir of infected cells shielded from the CTLs, reducing the selection pressure on the HIV replicating there. It provides an alternative or complementary explanation to those that have already been proposed to explain HIV's "slow" CTL escape during the chronic infection phase, and should be accounted for given that experiments have demonstrated the compartmentalised nature of secondary lymphoid tissues.

It has been observed that CTL escape mutants in people living with HIV arise faster during the acute phase of the infection, in contrast to the slow escape seen during chronic infection (61). During acute SIV infection, the distribution of virus across the follicular and extrafollicular compartments is more even than during chronic infection, due to less pronounced CTL activity (3). Hence, the compartmental dynamics that delay CTL escape mutant emergence in model (i) apply less during acute infection, potentialy explaining the discrepancy in the rate of escape mutant evolution. Thus, the compartmentalised model (i) can reconcile the relatively long emergence times for CTL escape mutants in chronic infection with the presence of a strong lytic CTL response that limits overall viral load. Simultaneously, the observed faster emergence of CTL escape in acute infection can be explained by lower escape times observed for weaker CTL responsiveness in model (i).

Chapter 5

Non-escape HIV mutant emergence

In this chapter, we now turn to looking at scenarios where HIV mutants are generated that do not escape the CTL response, but instead the mutations affect the infectivity (β) of the virus. It will build on the tools (i.e. Gillespie simulations) and two-compartment model shown in the previous chapter, with some subtle but important differences, in order to investigate how compartmentalisation affects the evolutionary course of HIV in these scenarios. We will primarily be interested in two aspects of HIV's evolution in this scenario: the fixation time and the fixation probability.

5.1 Fixation & the Moran process

Fixation is the process of replacing an initially heterogeneous population with the offspring of one individual. (67) The *fixation probability* is the probability that the offspring of that one individual eventually dominates the whole population, instead of going extinct, while the *fixation time* is the time taken for this to occur. Kimura was the first to use the term "fixation" in his series of seminal papers applying concepts and methods from statistical

physics to population genetics, although Haldane, Wright, and Fisher all did work on fixation probability and time that precedes Kimura. (68) (69; 70; 71)

In the context of HIV and non-escape mutant emergence, it makes sense to ask what the fixation probability of a HIV mutant with an infectivity-advantageous mutation is. To help answer this, one can use the Moran model with selection, a relatively simple stochastic model where the total population N is fixed. (72; 73) Assume two populations of HIV-infected cells of different strains, Y and Y_1, with infectivities β and β_1, where β_1 is advantaged by the factor $r > 1$, i.e., $\beta_1 = r\beta$. At each step of the stochastic Moran process, one cell is chosen to reproduce and another to die, thus keeping the population fixed. Since the mutant Y_1 has a reproductive fitness advantage r, the probability that Y_1 is chosen to reproduce is:

$$P_{Y_1 \to Y_1+1} = \frac{rY_1}{rY_1 + N - Y_1}.$$

The probability that wild type Y is chosen for reproduction is:

$$P_{Y \to Y+1} = \frac{N - Y_1}{rY_1 + N - Y_1}.$$

Conversely, since the reproductive fitness does not play a role in the death process, the probabilities that Y and Y_1 are chosen for death are, respectively:

$$P_{Y \to Y-1} = \frac{N - Y_1}{N},$$

$$P_{Y_1 \to Y_1-1} = \frac{Y_1}{N}.$$

The fixation probability of a single mutant in the population advantage r is (73):

$$\rho = \frac{1 - 1/r}{1 - 1/r^N}. \tag{5.1}$$

For very large N, then $\rho \sim 1 - 1/r$. The rate of evolution R from an all Y population to all Y_1 is given by:

$$R = N\mu\rho,$$

where μ is the mutation rate.

However, the Moran process assumes a *fixed* total population. In the case of HIV infection, it is clear that the total HIV-infected cell population is certainly not fixed, for it is subject to not only natural "birth" (cell infection) and death processes, but also to "predation" by the CTL response. These create fluctuations in the total infected cell population, as seen in the Lotka—Volterra predator-prey model. These can have a significant impact on evolutionary dynamics, as in Gokhale et al.'s work in host-parasite coevolution. (74)

There have been attempts to investigate the fixation probability of a mutant emerging in a varying population. Ewens derived the fixation probability of a favourable mutant emerging in population that cycles through a sequence of population sizes $N_1, N_2, N_3, ..., N_k, N_1, ...$ through a Moran-like process. (75) For a mutant with fitness advantage $1+\delta$, Ewens deduced that the fixation probability of the mutant in the cyclical population model was:

$$\rho = \frac{2\delta N^*}{\overline{N}},$$

where $\overline{N} = \sum_{i=1}^{k} N_i/k$ is the arithmetic mean while N^* is the harmonic mean:

$$N^* = k\left(\sum_{i=1}^{k} {N_i}^{-1}\right)^{-1}.$$

For a given $\overline{N}$ and k, the fixation probability is maximised when $N_1 = N_2 = ... = N_k$, whereupon $\rho = 2\delta$. Ewens noted that if the variation in the N_is is large, the fixation probability can be much lower than 2δ. Otto & Whitlock also found that this fixation probability

formula derived by Ewens is a good approximation for scenarios where the mutant emerges other cyclical populations such as those following a sinusoidal or log-sine function (76).

More recently, it was shown by Parsons & Quince that a similar suppression of mutant fixation probability also occurs in populations that intrinsically fluctuate stochastically (77). This is in contrast to the work of Ewens and Otto & Whitlock, where the fluctuations created artificially by forcing the populations through a cyclic pattern, and suggests that this effect is inherently caused by any variations in the population, regardless of the cause of the fluctuations, be they externally imposed by the environment or intrinsic random fluctuations.

Based on the results of Ewens, Otto & Whitlock, and Parsons & Quince, one can expect that the fluctuations of the HIV-infected cell population will result in a lower fixation probability than would be predicted by the Moran formula (5.1). One would also expect that the larger fluctuations are in the population, the greater the reduction in the fixation probability as well.

5.2 Non-escape HIV mutant emergence model

The deterministic mathematical models used for the non-escape mutant emergence scenario are similar to the ones used in Chapter 2 for a CTL escape scenario ((4.1) and (4.3)). However, here neither strain evades the CTL response. To simplify things, assume the CTL response strength parameter c is identical for both strains. The CTL response to the mutant strain with the populations Z_{1e} and Z_{1f} (only Z_1 in the single-compartment model) is completely independent of the CTL response to the wild strain (Z_e, Z_f).

The mutant emergence scenario can be described by the following system of deterministic ODEs for the single-compartment (Model I) case:

$$
\begin{aligned}
\dot{X} &= \lambda - dX - \beta XY - \beta_1 XY_1, \\
\dot{Y} &= \beta(1-\mu)XY - aY - pYZ, \\
\dot{Y_1} &= \beta\mu XY + \beta_1 XY_1 - aY_1 - pY_1Z_1, \\
\dot{Z} &= cY - bZ, \\
\dot{Z_1} &= cY_1 - bZ_1.
\end{aligned} \tag{5.2}
$$

This gives the required properties, where the CTL responses are equally effective against each strain, but are independent of each other. This is biologically realistic because CTLs undergo differentiation and are primed against a specific antigen. A CTL response against one strain may not recognise a different one. (78)

The two-compartment (Model II) case is given by the following system of ODEs:

$$
\begin{aligned}
\dot{X_e} &= \lambda - dX_e - \beta X_e Y_e - \beta_1 X_e Y_{1e}, \\
\dot{Y_e} &= \beta(1-\mu)X_e Y_e - aY_e - pY_e Z_e - \eta(Y_e - Y_f), \\
\dot{X_f} &= \lambda - dX_f - \beta X_f Y_f - \beta_1 X_f Y_{1f}, \\
\dot{Y_f} &= \beta(1-\mu)X_f Y_f - aY_f - pY_f Z_f - \eta(Y_f - Y_e), \\
\dot{Y_{1e}} &= \beta\mu X_e Y_e + \beta_1 X_e Y_{1e} - aY_{1e} - pY_{1e}Z_{1e} - \eta(Y_{1e} - Y_{1f}), \\
\dot{Y_{1f}} &= \beta\mu X_f Y_f + \beta_1 X_f Y_{1f} - aY_{1f} - pY_{1f}Z_{1f} - \eta(Y_{1f} - Y_{1e}), \\
\dot{Z_e} &= cY_e - bZ_e - gZ_e + hZ_f, \\
\dot{Z_f} &= gZ_e - bZ_f - hZ_f, \\
\dot{Z_{1e}} &= cY_{1e} - bZ_{1e} - gZ_{1e} + hZ_{1f}, \\
\dot{Z_{1f}} &= gZ_{1e} - bZ_{1f} - hZ_{1f}.
\end{aligned} \tag{5.3}
$$

Unless otherwise noted, the base parameter values used are given in Table 5.1. The reasoning behind these parameter values was already discussed in Chapters 2, 3, and 4. The c values in the single-compartment model are chosen so that the starting equilibrium infected cell population Y in the single-compartment model is equal to the initial total $Y_e + Y_f$ population in the corresponding two-compartment model.

Parameter table (non-escape HIV mutant fixation model)		
Parameter	Value/Range	Reference
Uninfected cell birth rate, λ	500	(22; 23; 18).
Uninfected cell death rate, d	0.01	(20; 21)
Infected cell death rate, a	0.45	(19)
Contact infection rate, β	7×10^{-5}	$R_0 = \beta\lambda/ad \approx 8$. (18; 19; 25)
Contact infection rate (mutant), β_1	1.005β or 1.01β	Plausible fitness advantages.
CTL killing rate, p	0.05	(48; 51)
CTL death rate, b	1	(52)
CTL expansion rate, c	10^{-3}–10	(49)
Infected cell migration rate, η	0.0001	(49)
CTL migration rate (EF to F), g	0.0001	(49)
CTL migration rate (F to EF), h	1	(49)
Mutation rate, μ	2×10^{-5}	(55)

Table 5.1: Table of parameters for non-escape HIV mutant fixation model.

The biologically realistic equilibria of these systems are:

- Extinction of both strains (stable when the $R_0 < 1$ for both strains).
- One strain dominates (i.e., mutant fixates or goes extinct).

In general, assuming both strains have $R_0 > 1$, the dominant strain is determined by the criterion $\beta - (\mu\beta + \beta_1)$, similar to the escape models in Chapter 2. If $\beta - (\mu\beta + \beta_1) > 0$, then the wild strain remains dominant and the mutant never fixates. Conversely, if $\beta - (\mu\beta + \beta_1) < 0$, then the mutant strain will fixate and displace the wild type into extinction. Because the CTL response is equally effective against both the wild and mutant strains, there is no coexistence equilibrium in the no-escape fixation scenario.

As noted in Chapter 4 as well, because mutation is fundamentally a probabilistic process and the models evolve from initially small mutant populations, it is more appropriate to model the non-escape fixation scenario using the stochastic Gillespie process. The same basic parameter values specified for the ODEs were used for the simulations. These simulations were then used to determine the average fixation times and fixation probabilities of the advantageous HIV mutant in the single and two-compartment models for various CTL response strengths and fitness advantages.

Once again, in Model I, λ is set to twice its value in Model II in order to maintain the same rate of generating uninfected cells, while β and β_1 are set to half their respective values in order to preserve $R_0 \sim 8$, as observed experimentally. To ensure a proper comparison between Models I and II, the parameter c for Model I is chosen so that the initial total wild-type infected cell population of Model I is the same as for the corresponding Model II for a chosen value of c there. As in Chapter 2, each Gillespie simulation run is done with an initial state where the wild strain-infected cell, uninfected cell, and CTL populations are in equilibrium with no mutants present, calculated using the deterministic equations (5.3) for the two-compartment scenario and (5.2) for the single-compartment one, rounded to the nearest integer. Each run is then allowed to evolve until the mutant fixates, defined as reaching 100% of the total population (across both compartments in the two-compartment scenario). The time between the start of the run and the end of fixation is taken to be the *fixation time*. Many runs are needed in order to get reasonably accurate statistics, usually $\sim 10^5$ runs. The fraction of runs in which the mutant first emerges in in the follicular (F) or extrafollicular (EF) compartments is also noted.

The *fixation probability* is defined as the probability that the offspring of a single mutant will fixate within the population. The Moran formula (5.1) gives the probability for a single mutant within a fixed-size population, which serves as the baseline for comparison. However, the population size is not fixed in both the single and two-compartment HIV models, thus

the Moran formula may not be accurate.

To simulate the fixation probability, the Gillespie simulations must be modified slightly. Instead of an initial zero-mutant population, a single mutant infected cell will be introduced at the beginning of the simulation run. In the two-compartment model (Model II), the location of this mutant will be determined by generating a random number r and comparing it to the criterion $Y_f/(Y_e + Y_f)$: if $r < Y_f/(Y_e + Y_f)$, then the mutant will be placed in the follicular compartment, otherwise it will be placed in the extrafollicular compartment. The mutation rate μ is set to zero, since only the descendants of the original mutant will be counted. The simulation is then run until either the mutant infected cells go extinct or they fixate, reaching 100% of the total population. If they do fixate, then the conditional fixation time is also recorded. The fraction of runs with fixation compared to the total number of runs is thus the fixation probability of the mutant strain.

Because the fixation probability is very low (the Moran formula (5.1) predicts the fixation probability to be between 9% to 0.5% depending on how advantageous the mutation is), a lot of runs are needed to obtain reasonably good statistics. For this work, it was found that at least $1,000,000$ runs are needed to obtain a reasonable number of runs where fixation occurs and thus statistically reasonable results, and sometimes significantly more are needed for the lower fixation probabilities.

5.3 Results & analysis

The fixation time results for $\beta_1 = 1.005\beta$ and $\beta_1 = 1.01\beta$ with mutation are shown in Fig. 5.1. Fig. 5.2 shows how the initial follicular, extrafollicular, and total infected cell populations change as c is varied.

The results for both values of β_1 show similar behaviour when the CTL response strength

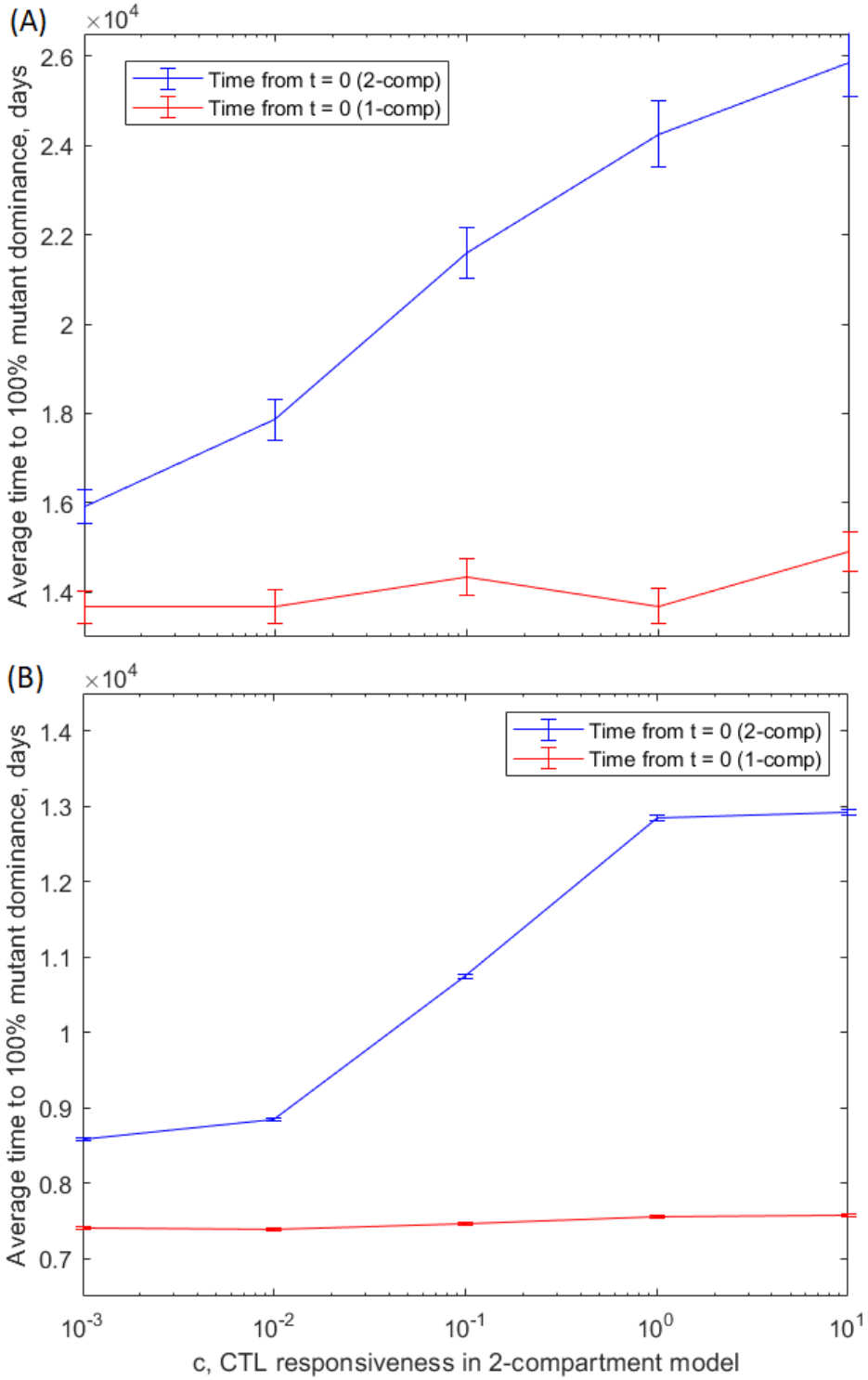

Figure 5.1: Fixation times for (A) $\beta_1 = 1.005\beta$ and (B) $\beta_1 = 1.01\beta$ given various values of c given various values of c for the two-compartment (blue) and one-compartment (red) models. The error bars show the standard error.

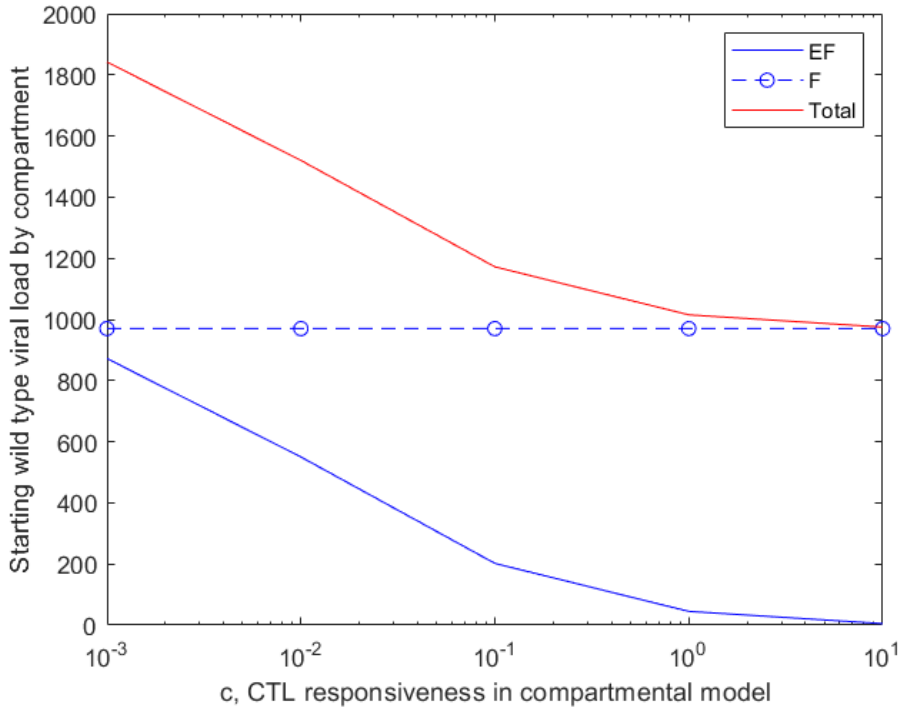

Figure 5.2: Initial F (blue dashed), EF (blue), and total (F + EF, red) wild type populations in the two-compartment model given various values of c. The single-compartment model's parameters are chosen so that it has the same populations as the corresponding two-compartment model's total populations.

c is varied. In the two-compartment model, the lowest fixation time is observed for low values of c, and the fixation time increases as c increases. For $\beta_1 = 1.01\beta$, the fixation time appears to plateau for $c > 1$ and $c < 0.01$, while for $\beta_1 = 1.005\beta$ it appears to increase more monotonously. Conversely, the fixation times of the single-compartment model appear to be fairly independent of c. It is quite clear that the compartmentalisation has a significant impact on the fixation process, but the question is: *how* exactly does compartmentalisation affect the fixation time, i.e., by what mechanism?

Mutant fixation is a combination of two processes: *mutant generation* (i.e., the time it takes for the mutant to be created) and *mutant invasion* (i.e., the time for the mutant to reproduce and displace the original population). Intuitively, one might surmise that as the total wild-type populations are decreases as the CTL response increases, the longer it will take to generate a mutant. After all, given a smaller population, the mutant generation rate ($\mu\beta Y$) will be lower for a fixed mutation rate and infectivity. This will tend to delay mutant creation.

However, if that were the sole reason, then we would expect the single-compartment's fixation times to follow the same pattern, since we chose c values so that it has the same total wild infected cells as the corresponding two-compartment model. This suggests that there are additional factors at play here.

Consider Fig. 5.3, which shows the fractions of compartments for the two-compartment model in which the mutant successfully first emerges before fixating for $\beta_1 = 1.01\beta$. It can be seen in Fig. 5.2 that, for lower c, the EF and F populations are comparable, and thus the fixating mutant is more-or-less equally likely to appear in either compartment. At higher c, the EF population is much lower, since the CTL response is stronger there, hence the fixating mutant is far less likely to appear in the EF compartment first. This is in clear contrast to the pattern observed in Chapter 4 (c.f. Fig. 4.7 (C)), where the mutant preferentially appears in the EF compartment first due to its ability to evade the CTL response. The F

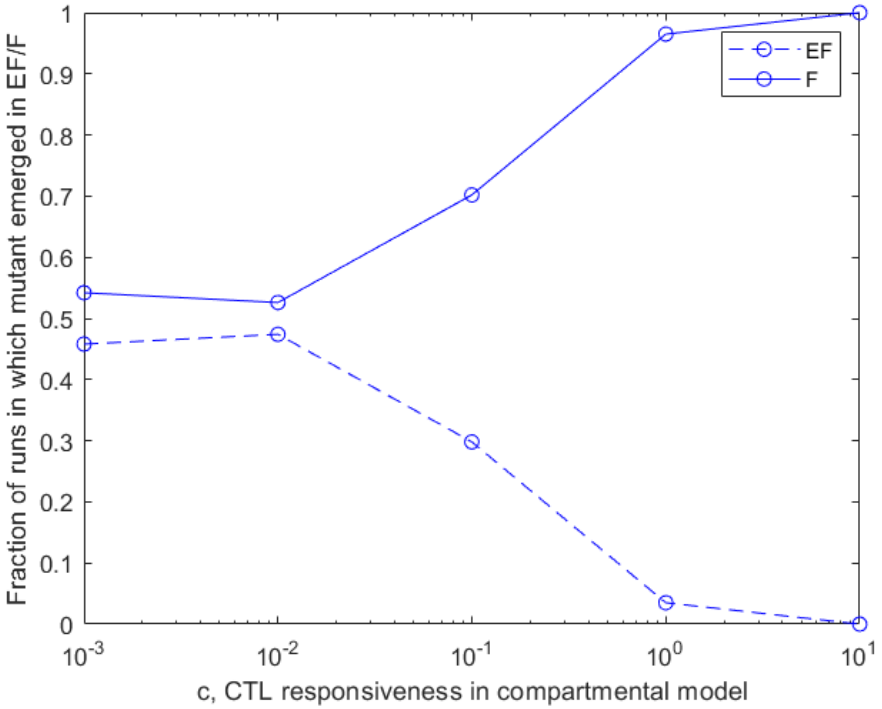

Figure 5.3: Fraction of runs in which the fixating mutant first emerged in EF (dashed) or F (solid) for $\beta_1 = 1.01\beta$ given various values of c.

compartment is shielded from the CTL response, thus decreasing the selective pressure and infected cell turnover. This means that the CTL escape mutant has less of an advantage in F compartment, hence why it preferentially emerges in the EF compartment. However, here the mutant does not directly evade the CTL response: it has a higher infectivity than the wild type, which is a selective advantage in either compartment. This makes it unlikely that the CTL response is completely responsible for the behaviour.

It is interesting to look at what happens if the mutation rate is increased. Fig. 5.4 shows the fixation times for mutation rates $\mu = 5 \times 10^{-5}$ (A) and 2×10^{-3} (B) with $\beta_1 = 1.01\beta$. At lower mutation rates, it is natural to expect that the fixation times will increase as c increases, since it will take longer to generate a mutant due to the shrinking population from the CTL response. However, the disproportionate effect that increasing c has on the two-compartment model suggests that some other factors are at play here. Notably, the

fixation times for higher c are significantly greater for the two compartment model than the one-compartment model. This pattern is robust across the different mutation rates.

Let us consider what are the main differences between the two models:

- Uneven CTL response, with a strong response in EF and nearly none in F, for the two-compartment model, while a uniform but weaker response in the one-compartment model, required to keep the total population sizes the same for both models.
- Smaller initial wild-infected cell population size of the EF compartment compared to F in the two-compartment model, ranging from around 870 at $c = 0.001$ to 6 at $c = 10$ for the former, while F remains mostly fixed at around 970 for all c values. In the one compartment model, the total population size decreases from around 1840 to 970.
- The need for infected cells to migrate into both compartments for fixation to occur in the two-compartment model due to their compartmentalisation.

The CTL response is equally effective against both strains and the infectivity advantage is equally selected for in both compartments, so the CTL response alone cannot explain the diverging fixation times. This leaves us with the other two possibilities.

The changing population sizes have two effects:

- A smaller population size decreases the mutant generation rate for given a fixed mutation rate.
- Fixation occurs faster in a smaller population, since it will take less time for the mutant to reproduce to reach 100% of the population than in a larger population.

These two effects act in opposite directions (one tends to increase the overall fixation time by the reducing mutant generation rate, while the other decreases it by reducing the mutant

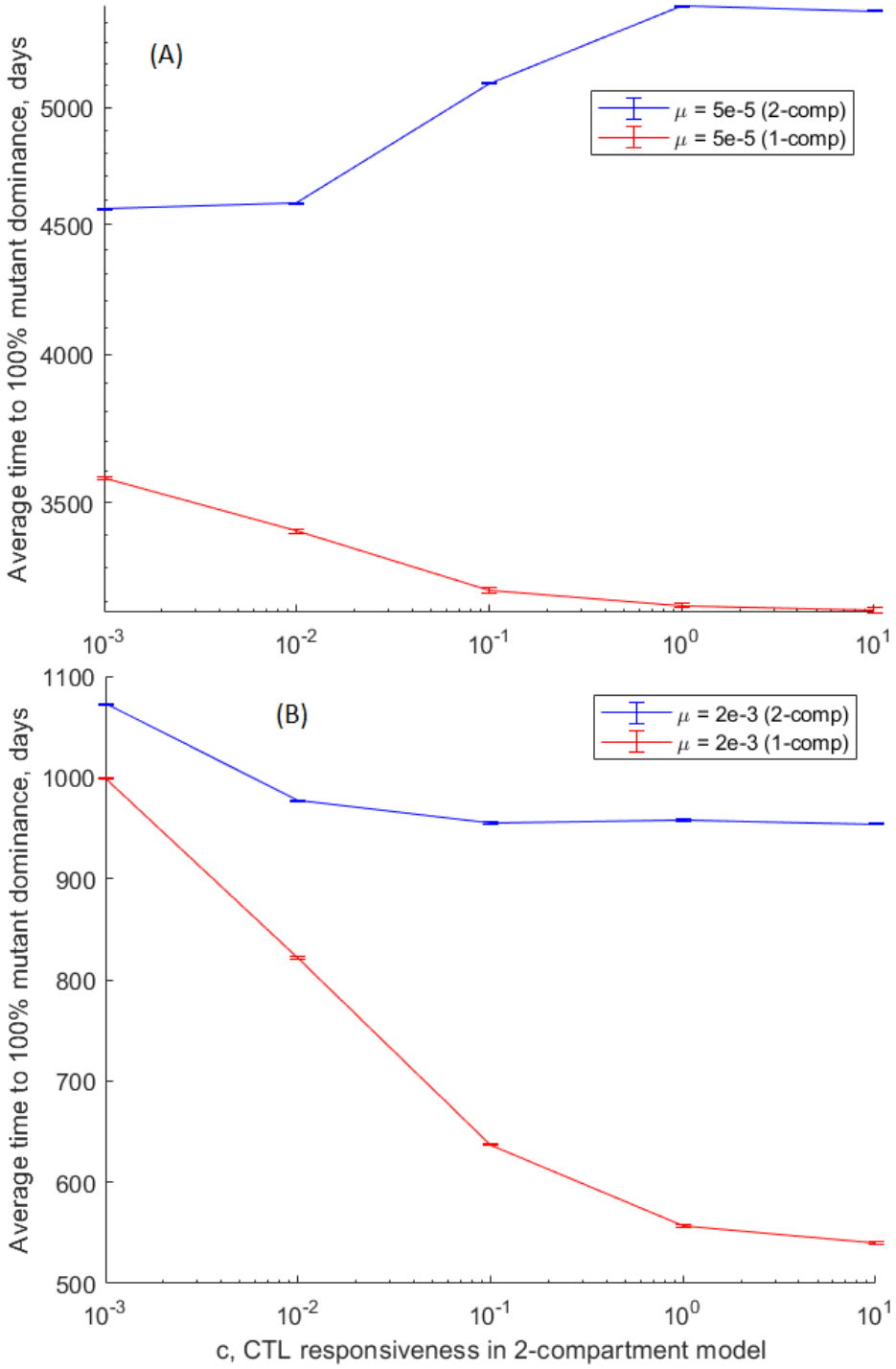

Figure 5.4: Fixation times for $\beta_1 = 1.01\beta$ given various values of c, (A) $\mu = 5 \times 10^{-5}$ and (B) $\mu = 2 \times 10^{-3}$ for the two-compartment (blue) and one-compartment (red) scenarios. The error bars show the standard error.

invasion time) as c increases. However, the population size effect alone is insufficient to explain the disparity in fixation time observed between the two models for larger c for the various mutation rates, especially in the case $\mu = 2 \times 10^{-3}$, where the mutation rate is high enough so that a mutant is generated very quickly from the initial populations.

By exclusion, this leaves us with the third factor, the compartmentalisation itself. We defined fixation as the process of the mutant completely displacing 100% of the initial wild-type population. This means that the mutant has to displace the wild strain in *both* compartments of the two-compartment model. We can see that in Fig. 5.3, as c increases the virus preferentially emerges in the F compartment due to the majority of the wild infected cells being killed in the EF compartment, thus having a much smaller population.

A mutant emerging in F must then migrate to the EF compartment in order to fixate, but this is limited by the very small migration rate $\eta = 0.0001$. This could serve as a bottleneck that could explain why the fixation time for the two-compartment model diverges from that of the one-compartment model with increasing c for all μ. It is known from mathematical studies that, in subdivided populations, the migration rate between the population groups is inversely related to the fixation time for an advantageous mutant in the Moran birth-death process (79; 80; 81; 82). This provides further support for the migration rate hypothesis.

Furthermore, in the EF compartment, the death rate of infected cells is very high because of the strong CTL response at high c. A mutant-infected cell migrating from F to EF is likely to be killed before it can spread. This further decreases the already low probability of the mutant to invade into the EF compartment and can significantly delay complete fixation in both compartments for large c.

We now turn to the matter of the fixation probabilities. Fig. 5.5 shows the fixation probabilities for the β_1 ($\beta_1 = 1.005\beta, 1.01\beta$) and c values considered in Fig. 5.1. Here, $\mu = 0$, since we are only interested in the probability that the only starting mutant's offspring fixate, and

the red dashed line in each graph shows the predicted fixation probability using the Moran formula (5.1) based on the total population. Fig. 5.6 presents the conditional fixation times corresponding to Fig. 5.5.

The conditional fixation time graphs for both parameter sets show consistent behaviour: monotonous decline in the fixation time as c increases. In all both cases, the two-compartment's fixation times are universally significantly greater than those of the single-compartment. Once again, this discrepancy between the two models suggests that the behaviour cannot be solely explained by the fact that the total infected cell population is decreasing as c increases, since both models have the same total populations. Since the mutation rate is set to zero and the simulations already start with a single mutant, the discrepancy cannot also be attributed to the time it takes for a mutant to appear, as might be concluded from Fig. 5.1. It is therefore strongly indicative that the compartmentalisation of the CTL response is the cause of the difference, which supports the conclusions obtained from Fig. 5.4.

The behaviour of the fixation probability graphs in Fig. 5.5 is rather more interesting, but also difficult to interpret. The fixation probabilities in both models are universally lower than the ones calculated using the Moran formula, as predicted earlier due to the population fluctuations induced by CTL "predation." Due to the low fixation probabilities involved (for example, based on the Moran formula, the number of runs that would be expected to reach fixation given $\beta_1 = 1.01\beta$ is only $\sim 10,000$ out of $1,000,000$ runs, and even less for $\beta_1 = 1.005\beta$. This results in a considerable degree of statistical uncertainty.

One pattern that can be noticed in the graphs is, in the two-compartment model, after an initially high fixation probability for low c, the probability decreases as c increases until it reaches a certain point, where it begins to increase again along with c. In the cases of $\beta_1 = 1.01\beta$ (Fig. 5.5 (B)), the fixation probability at $c = 10$ is even higher than for $c = 0.001$.

One possible explanation is that fluctuations in the infected cell populations induced by the

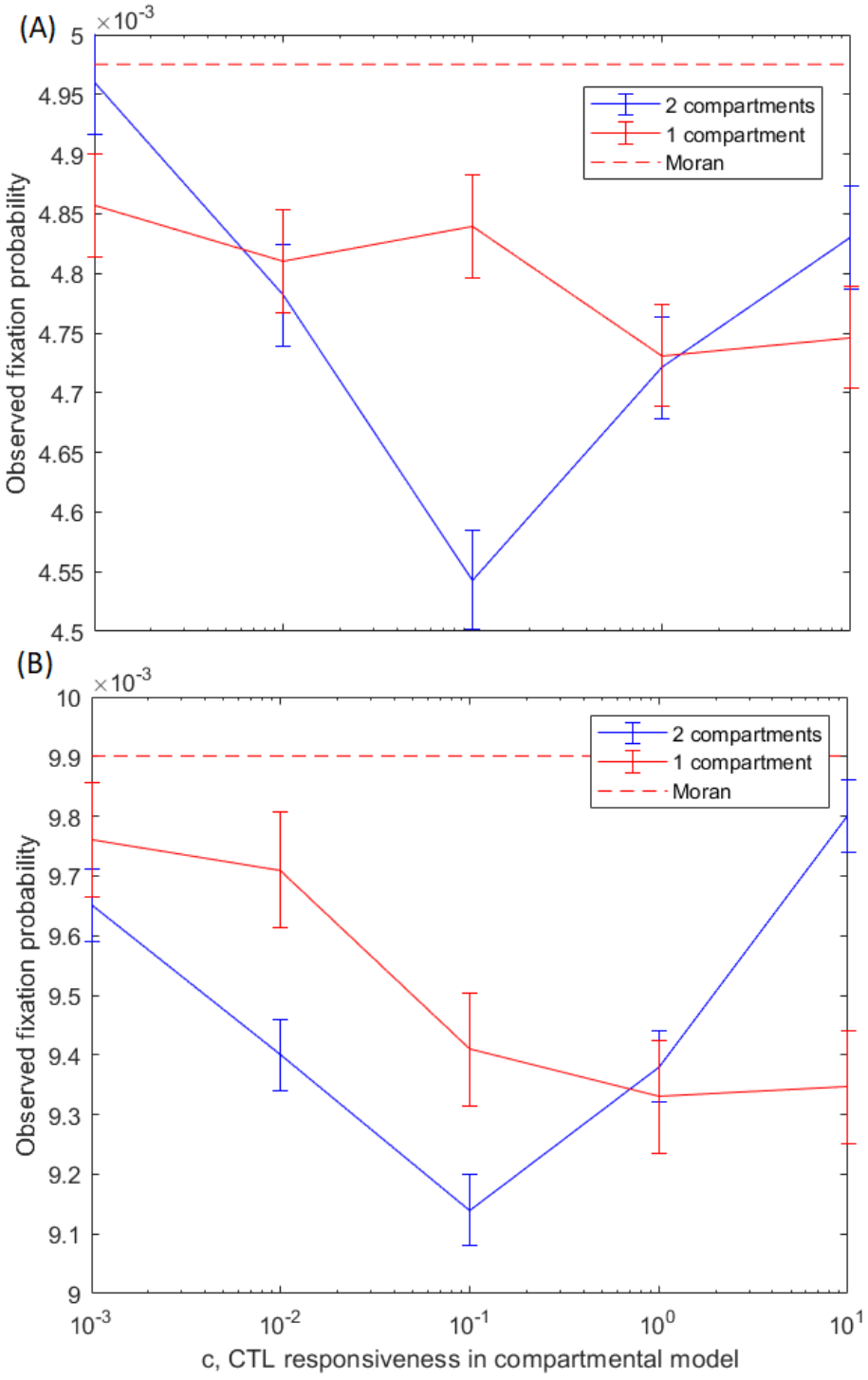

Figure 5.5: Fixation probabilities for (A) $\beta_1 = 1.005\beta$ and (B) $\beta_1 = 1.01\beta$ given various values of c and μ in the two-compartment (blue) and the one-compartment (red) scenarios. The error bars show the standard error at the 95% confidence interval.

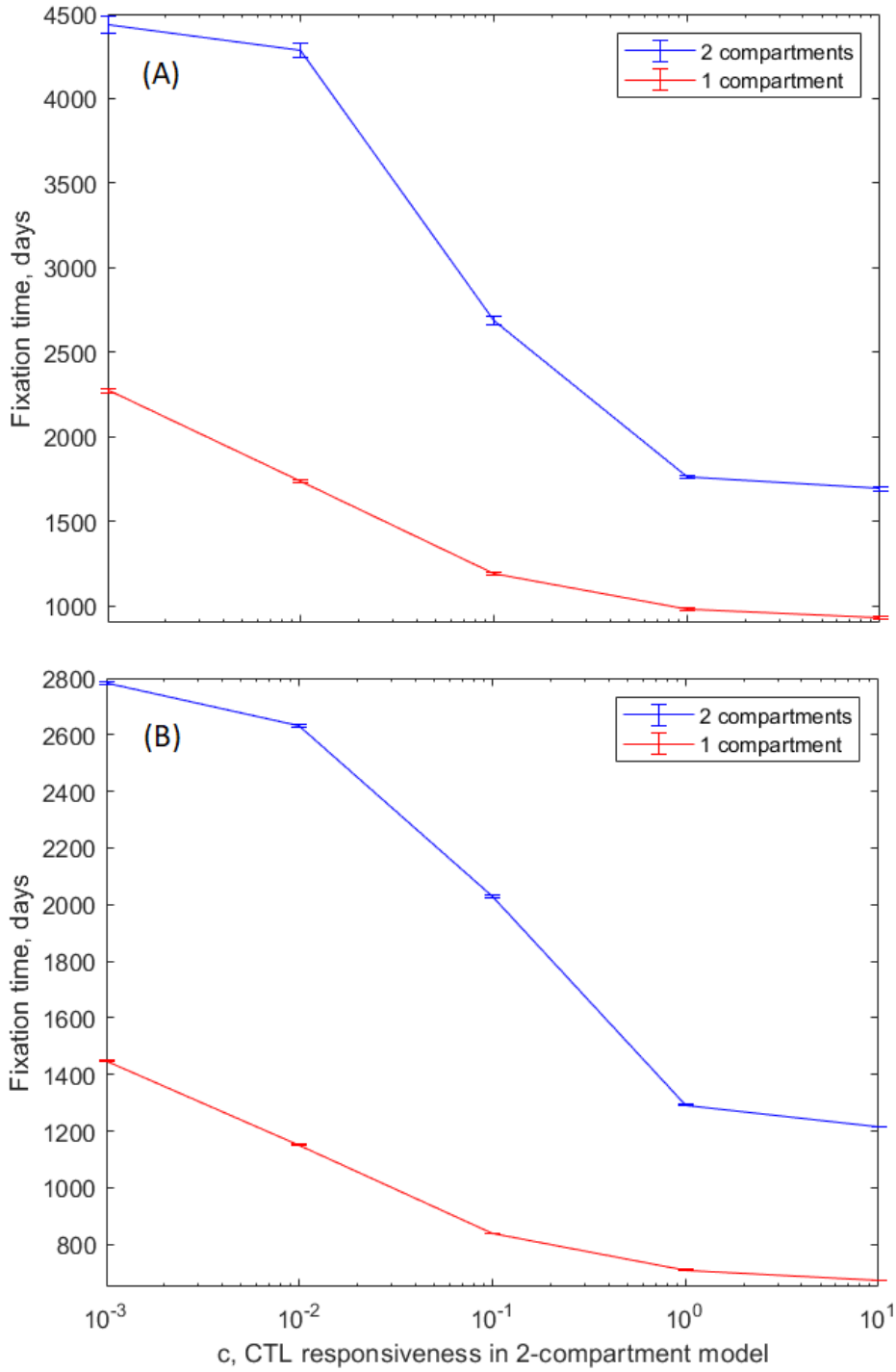

Figure 5.6: Conditional fixation times for (A) $\beta_1 = 1.005\beta$ and (B) $\beta_1 = 1.01\beta$ given various values of c and μ in the two-compartment (blue) and the one-compartment (red) scenarios.

CTL response are affecting the fixation probability. At lower c, the CTL response is weak and does not induce many fluctuations. Higher c induces larger fluctuations, decreasing the fixation probabilities. This alone could explain the relatively consistent decrease in the fixation probability as c increases in the single compartment model. Another factor that needs to be considered is the impact of the population sizes themselves on the fixation probability. In the two-compartment model, as the CTL response gets stronger, the fluctuations in the EF compartment increase, but the EF population also gets smaller, becoming minuscule in comparison to the F compartment. The F compartment, on the other hand, is mostly unaffected by the CTL response, and as the EF population shrinks, it is the dynamics in the F compartment that become dominant. This might explain the "V"-shaped curve in the fixation probabilities for the 2-compartment model.

To gain some insight into these, simulations were done with different uninfected cell production rate λ values ($\lambda = 50, 500, 5000$, with $\beta = 7 \times 10^{-4}, 7 \times 10^{-5}, 7 \times 10^{-6}$ scaled accordingly to maintain the reproduction number $R_0 \sim 8$ and $\beta_1 = 1.01\beta$). This results in significantly smaller ($\lambda = 50$) or larger ($\lambda = 5000$) infected cell populations than the baseline $\lambda = 500$ value. The fixation probability results are presented in Fig. 5.7 ($\lambda = 50$ and 5000). The reader may refer to Fig. 5.5 (B) for the baseline ($\lambda = 500$) graph. Once again, $\mu = 0$, since we are only interested in the probability that the sole starting mutant's offspring fixate, and the red dashed line in each graph shows the predicted fixation probability using the Moran formula (5.1), based on the total populations. It is noteworthy in the $\lambda = 50$ case that the Moran predicted fixation probability is increasing with c. This is because the populations (N) involved are small enough that $1/r^N$ in the denominator in the formula is no longer negligible. Therefore, as the CTL response grows stronger, the infected cell population shrinks, resulting in the denominator $(1 - 1/r^N)$ decreasing. Since the numerator $(1 - 1/r)$ is fixed, the predicted fixation probability increases.

The relative size of the fluctuations can be measured using the standard deviation normalised

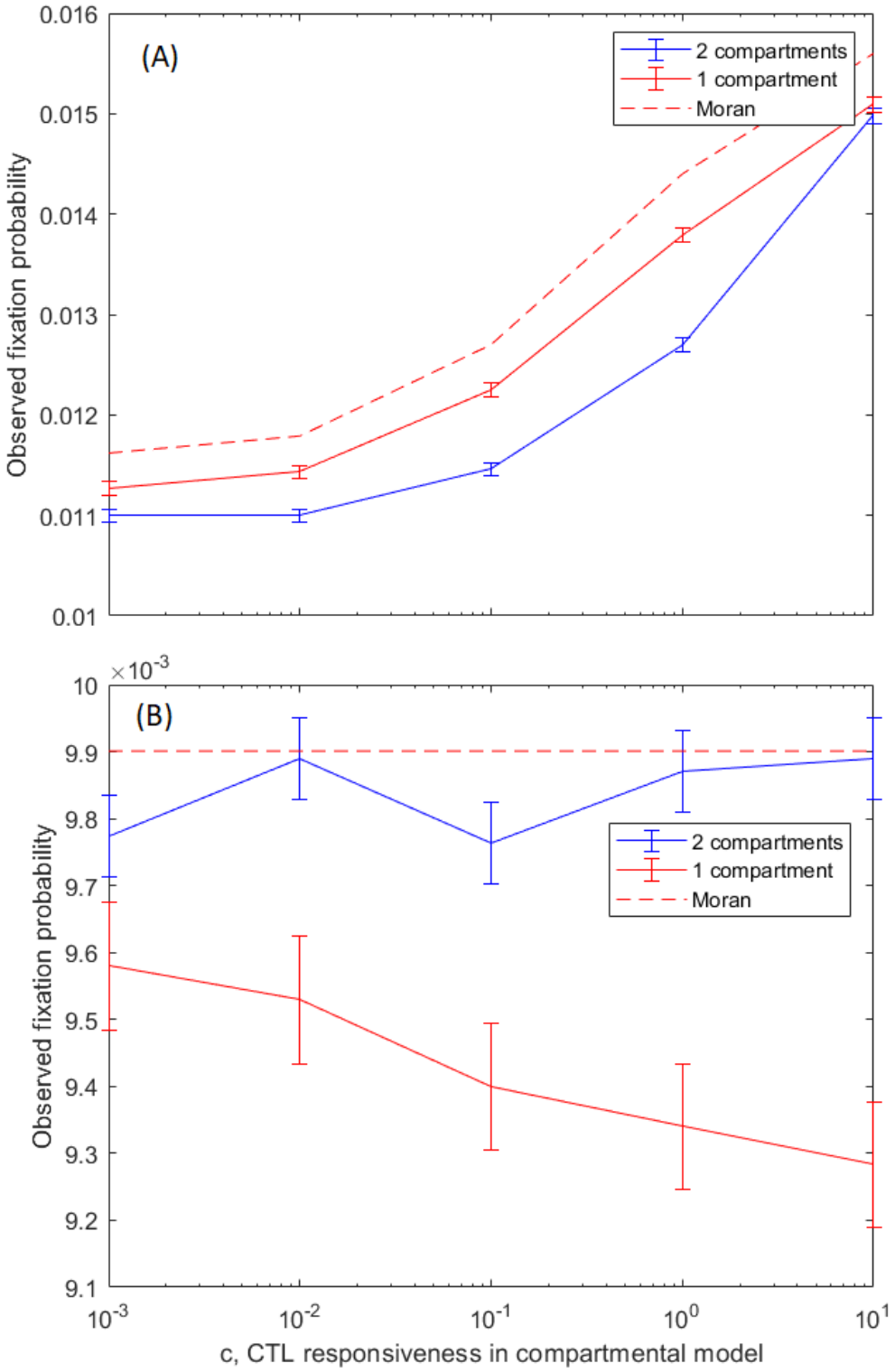

Figure 5.7: Fixation probabilities for $\beta_1 = 1.01\beta$ and (A) $\lambda = 50$ and (B) $\lambda = 5000$ given various values of c in the two-compartment (blue) and the one-compartment (red) scenarios. The error bars show the standard error at the 95% confidence interval.

by the (arithmetic) mean of the infected cell populations. This is shown for $\lambda = 50, 5000$ in Fig. 5.8. It can be clearly seen that as the CTL response gets stronger, the standard deviation/mean ratio (and therefore the relative size of the fluctuations) increases. This is driven both directly via the strengthening CTL response itself and indirectly via the decreasing infected cell population caused by the former. It is also apparent that the follicular infected cell population (Y_f) in the two-compartment model is barely affected by the strengthened CTL response due to the compartmentalisation.

Earlier in the chapter, Ewens' work showing that cyclical fluctuations reduce fixation probability was described. It is reasonable to regard a cyclically fluctuating population as a good approximation for the CTL-induced fluctuations of the HIV infected cell populations. Using the ratio of the infected cell populations' harmonic means to their arithmetic means (denoted $N^*/\overline{N}$), as Ewens did for cyclic populations, Fig. 5.9 shows how it changes with c for $\lambda = 500$ together with the standard deviation/arithmetic mean ratio. It is inversely related to the standard deviation/mean (i.e., the relative fluctuation size). This provides support for the relationship between Ewens' results for fixation probability in a cyclical population and the behaviour we are seeing in Fig. 5.5. The harmonic/arithmetic mean ratio $N^*/\overline{N}$ for the combined $Y = Y_e + Y_f$ population will not give an accurate picture of the dynamics of the system as a whole, since the F and EF compartments have very different CTL responses and thus fluctuations.

Paying particular attention to the $\lambda = 500$ case and comparing it to the population fractions shown in Fig. 5.2, this appears to be consistent with the explanation proposed earlier for the "V" shape curve of the two-compartment model's fixation probabilities in Fig. 5.5 (B). For lower c, the mutant is relatively equally likely to appear in either the EF or F compartments, and since the overall CTL response is weak in both compartments, the fluctuations are small in both compartments. This would increase the overall fixation probability. As the c increases, the fluctuations increase for the EF population, which would lower the overall

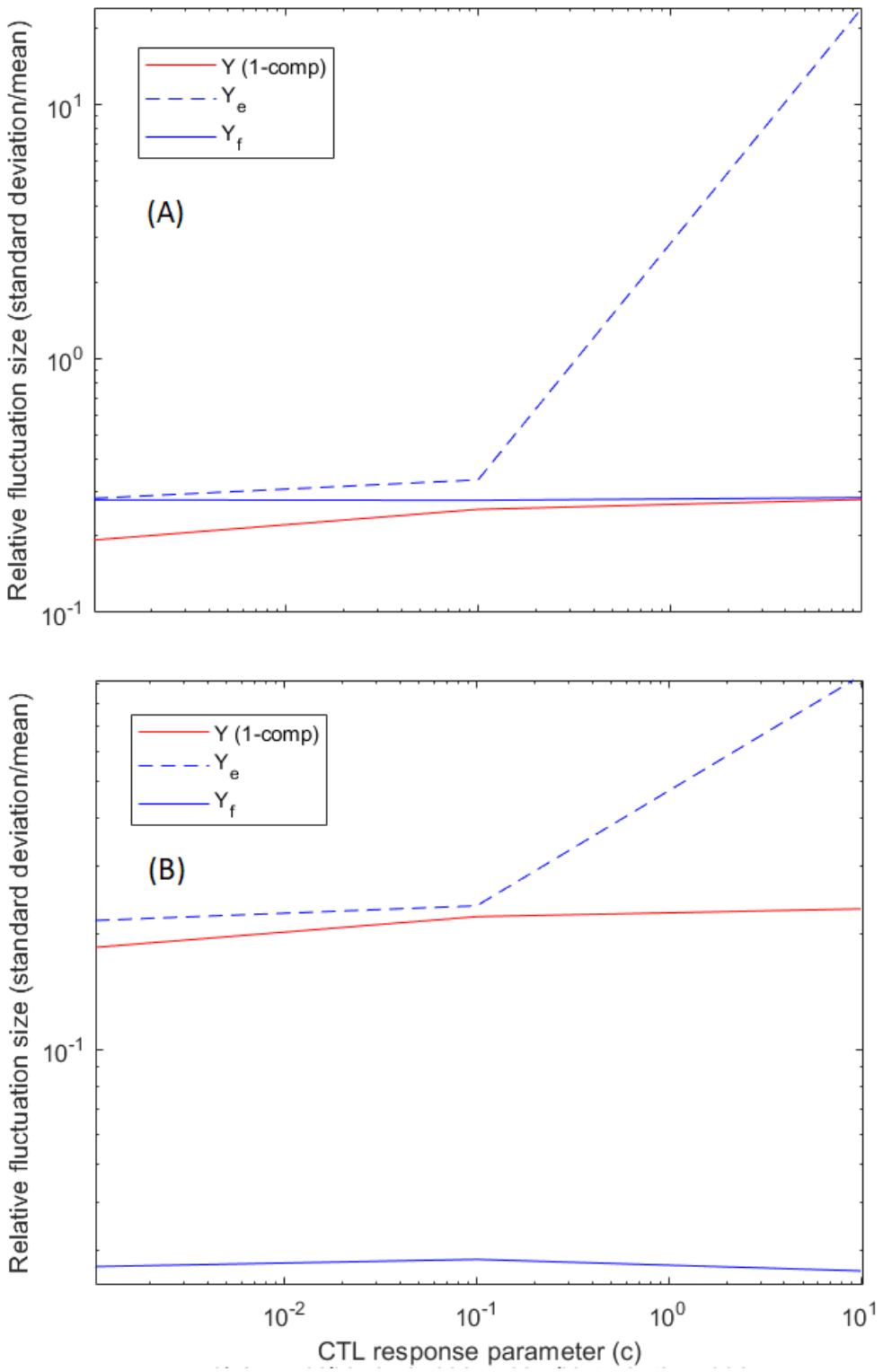

Figure 5.8: Standard deviation/arithmetic mean for the wild infected cell populations at equilibrium with (A) $\lambda = 50$ and (B) $\lambda = 5000$ given various values of c in the two-compartment (blue) and the one-compartment (red) scenarios.

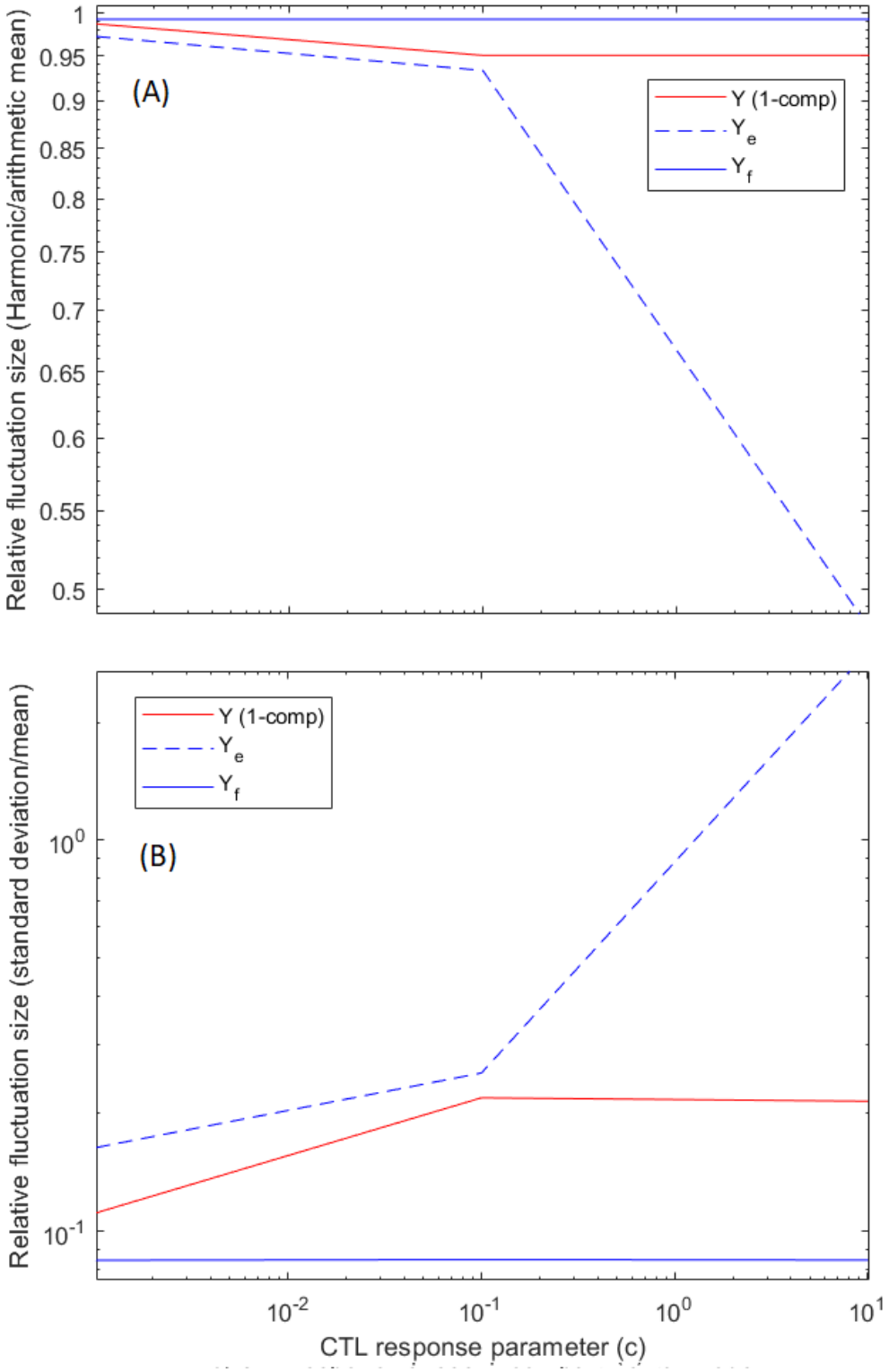

Figure 5.9: (A) Harmonic mean/arithmetic mean and (B) standard deviation/arithmetic mean for the wild infected cell populations at equilibrium with $\lambda = 500$ given various values of c in the two-compartment (blue) and the one-compartment (red) scenarios.

fixation probability. However, the EF population is also decreasing, and it becomes less likely for a mutant to spawn there. The F compartment, on the other hand, is mostly unaffected by the CTL response, and as c continues to increase , it is the dynamics in the F compartment that become dominant. At very high c, the EF population is too small to significantly affect the fixation probability, hence it would be almost completely driven by the population dynamics in F.

To further cement this, we can look at what happens if we reduce c and b by a factor of 100. Doing so does not affect the initial equilibrium populations, but significantly increases the relative size of the fluctuations. This can be seen in Fig. 5.10 for $\lambda = 500$ and 5000. It can clearly be seen that the relative fluctuation sizes as measured by the standard deviation/mean ratio are significantly higher than in Figs. 5.8 (B) and 5.9 (B).

The fixation probability simulations for $\lambda = 500$ and $\lambda = 5000$ are given in Fig. 5.11. As predicted, the fixation probability is generally lower for both the single and two-compartment models, which can only be attributed to the increased fluctuation sizes: the selective advantage of the mutant remains fixed and the equilibrium infected cell population sizes are almost exactly the same. As seen in Figs. 5.5 (B) and 5.7 (B), in the two-compartment model, after decreasing because of increased fluctuations induced in the EF infected cell population, the fixation probability increases again after a certain point because the evolutionary dynamics of the much larger F compartment infected cell population become more dominant. As the EF compartment's infected cell population is reduced with the increasing CTL response, it becomes less and less relevant to the overall dynamics. This is what causes the fixation probabilities of the two-compartment model to converge towards the predicted by the constant-population Moran process. The single-compartment model's fixation probability decreases monotonously with increasing c, as expected, due to the increasingly larger fluctuations induced by the CTL response. These results, combined with those in Figs. 5.5 (B) and 5.7 (B), provide strong support for our hypothesis that fluctuations can explain

the unusual discrepancy in behaviour observed in the fixation probabilities of the single and two-compartment models.

In summary, HIV evolutionary dynamics concerning the fixation of an advantaged HIV mutant become significantly richer and more complex when transitioning from a single homogeneous compartment model to a two-compartment model where the CTL response is considerably more constrained in the follicular compartment compared to the extrafollicular compartment. The simulations implemented and shown in this work stress the importance of considering the following factors and how they balance against each other when dealing with fixation times and probabilities and how the compartmentalisation affects them:

- Differences in infected cell population sizes between the two compartments due to the uneven CTL response, and their effect on the mutant generation and invasion processes.
- CTL-induced fluctuations in the infected cell populations.
- The migration rate of infected cells between the two compartments.

The complex interplay between these factors significantly complicates the dynamics compared to those of the post-ART decline dynamics of Chapter 3 and CTL escape evolution in Chapter 4, and the author believes that further work examining HIV mutant fixation in a compartmentalised medium is highly warranted.

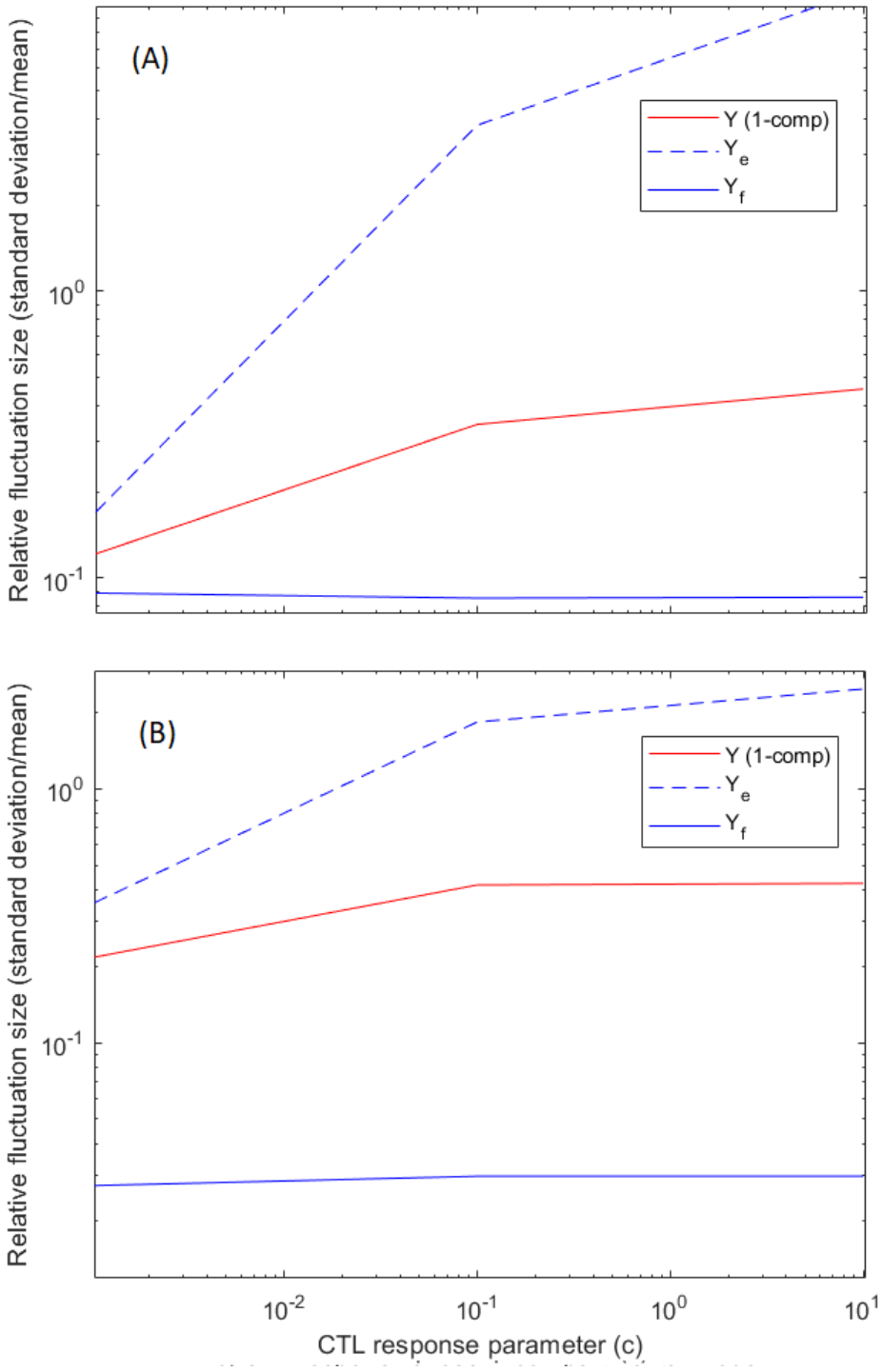

Figure 5.10: Standard deviation/arithmetic mean for the wild infected cell populations with (A) $\lambda = 500$ and (B) $\lambda = 5000$, with $b = 0.01$, given various values of c in the two-compartment (blue) and the one-compartment (red) scenarios.

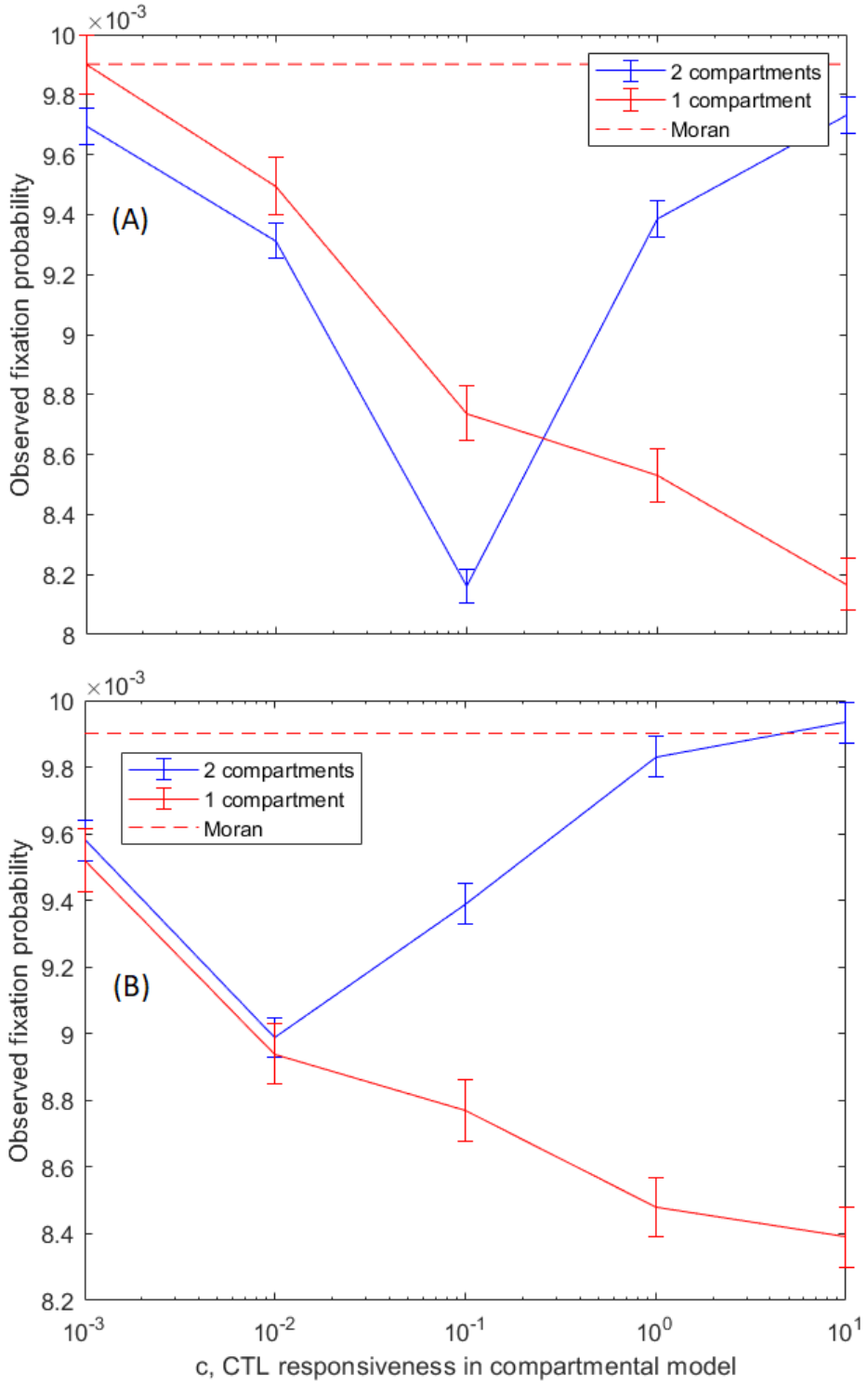

Figure 5.11: Fixation probabilities for $\beta_1 = 1.01\beta$ and (A) $\lambda = 500$ and (B) 5000 given various values of c in the two-compartment (blue) and the one-compartment (red) scenarios. Here, both c and b are divided by 100 within the model to increase the size of the fluctuations. The error bars show the standard error at the 95% confidence interval.

Chapter 6

Conclusion

Mathematical models have made major contributions to our understanding of HIV dynamics. Most are simplified models that treat the in vivo HIV population as a homogeneous, well-mixed system. Some studies have used more complex spatial models to explore viral dynamics, but explicit consideration of uneven virus replication and uneven CTL responses in the extra-follicular and follicular tissues of secondary lymphoid tissues has been largely neglected.

It is clear that incorporating the effects of compartmentalisation into mathematical models of HIV dynamics and evolution can dramatically alter the in vivo population and evolutionary dynamics of HIV. It can also help explain some puzzling observations that have been made about HIV dynamics and evolution with potentially clinically important consequences:

- Apparent lack of effect that CTL depletion has on post-ART SIV clearance in the SIV-simian experimental model of HIV infection.
- Slower-than-expected rate of escape for HIV against the CTL response during chronic HIV infection.

When applied to the scenario of non-escape advantageous HIV mutant fixation, it highlights the influence that HIV-infected cell population fluctuations induced by the uneven CTL response have on HIV's evolutionary dynamics. This is in addition to the direct effects from the uneven selection pressure already seen in the post-ART clearance and escape mutant evolution scenarios. It also highlights some of the more counter-intuitive aspects that emerge when compartmentalisation is taken into account in these models.

It is hoped that collaboration with experimental scientists will allow the parameters used in this model to be better estimated, which will greatly help in refining the compartmentalised models and confirming their predictions. In particular, the parameters g, η, and h governing the permeability of the compartments to CTLs and infected cells are not well-constrained, and experiments measuring the flow of CTLs and infected cells across the B-cell follicle barrier in a lymph node. The author envisages that such experiments would need to involve lymph node biopsies taken from both inside and outside the B-cell follicles of a lymph node over a period of time.

As discussed in Chapter 3, for the single-compartment model in the post-ART decline scenario, there is a point at which the post-ART decline rate for the total population of infected cells changes from being dominated by the CTL killing action to being dominated by the natural infected cell death rate as the infected cell and CTL populations decline over time. This point does not exist in the two-compartment model because the decline there is completely dominated by the much larger follicular compartment, where CTL action is minimal. Experimental measurements of post-ART HIV/SIV viral load over time can therefore help validate the two-compartment model by determining the existence of this point.

With respect to the HIV mutation (both escape and non-escape) scenarios, the author once again believes that the results of this theoretical work mean that future experiments to determine the rate of escape or mutant fixation should be based on measurements of mutant and wild viral loads taken from within the lymph node compartments, rather than from

peripheral blood. Time-series data of the viral loads can help validate the two-compartment model, however the author recognises the difficulty of obtaining these measurements. Nevertheless, the profound potential benefits that can be obtained from a better understanding of HIV dynamics in the lymph node and its impact on HIV evolution cannot be understated.

A potential direction for future theoretical work is investigating the effect of compartmentalisation in therapeutic contexts. We have already seen the effect of compartmentalisation on post-ART HIV clearance in Chapter 1. It was mentioned in that chapter that the issue of ART drug penetration into follicular lymphoid tissues is mostly unresolved, because while at least one study reported sub-optimal drug concentrations in the follicles, there is no evidence of ART-resistance emerging from the secondary lymphoid tissues during treatment. It will be interesting to see whether an uneven cross-compartment ART effectiveness can reconcile these apparently contradictory findings, as was possible in the post-ART clearance and slow CTL escape scenarios. Such a scenario can be modeled by having different infectivities (β_e and β_f) for each compartment; the work in this dissertation assumes that the infectivity is identical in both compartments.

In conclusion, the arguments and simulation results presented in this dissertation lead to the conclusion that, even though it adds some complexity to the mathematical models, compartmentalisation is a factor that should be considered for any mathematical model of the in vivo population and evolutionary dynamics of HIV. While it is considerably more difficult to mathematically analyse the two-compartment models compared to their single-compartment equivalents, the former may better encapsulate the essential population and evolutionary dynamics of HIV. Given that most HIV replication occurs in the secondary lymphoid tissues, observations of which confirm their compartmentalised nature, it might be important to investigate more closely the heterogeneity in virus dynamics between the follicular and extrafollicular compartments when studying the dynamics and evolution of HIV in vivo, rather than to solely concentrate on plasma viral loads measured in patients,

as is the usual method. It is admittedly more difficult to monitor viral loads in lymphoid tissues compared to the peripheral blood, especially in human patients, but as the work and mathematical models in Chapters 1 and 2 show, it may be a necessity in order to better understand how HIV infection actually progresses and evolves in the human body.

Chapter 7

Bibliography

[1] "Human immunodeficiency virus 1." ViralZone, Expasy Swiss Bioinformatics Resource Portal, https://viralzone.expasy.org/5182g (accessed June 13, 2023).

[2] The Science of HIV Project, www.scienceofhiv.org (accessed June 13, 2023).

[3] Connick E., Folkvord J. M., Lind K. T., Rakasz E. G., Miles B., Wilson N. A., Santiago M. L., Schmitt K., Stephens E. B., Kim H. O. et al. "Compartmentalization of SIV Replication Within Secondary Lymphoid Tissues of Rhesus Macaques is Linked to Disease Stage and Inversely Related to Localization of Virus-Specific CTL." J. Immunol. (2014); 193(11): 5613–5625. doi: 10.4049/jimmunol.1401161.

[4] Rambaut A., Posada D., Crandall K., and Holmes E. C. "The causes and consequences of HIV evolution." Nat. Rev. Genet. (2004) 5: 52–61. doi:/10.1038/nrg1246.

[5] Hellmuth J, Valcour V, and Spudich S. "CNS reservoirs for HIV: implications for eradication." J. Virus. Erad. (2015); 1(2): 67-71 (2015).

[6] Routy J. P., Dupuy F. P., Lin J., Isnard S. "More than a Gender Issue: Testis as a Distinctive HIV Reservoir and Its Implication for Viral Eradication." Methods Mol. Biol. (2022); 2407: 173-186. (2022) doi: 10.1007/978-1-0716-1871-4-13.

[7] Dahabieh M., Battivelli E., and Verdin E. "Understanding HIV Latency: The Road to an HIV Cure." Annu. Rev. Med. (2015); 66: 407–421. doi: 10.1146/annurev-med-092112-152941.

[8] Siliciano R. F. and Greene W. C. "HIV latency." Cold Spring Harbor perspectives in medicine (2011); 1(1): a007096. doi:10.1101/cshperspect.a007096.

[9] "HIV Treatment: The Basics." National Institutes of Health, www.hivinfo.nih.gov/understanding-hiv/fact-sheets/hiv-treatment-basics (accessed June 13, 2023).

[10] Jensen B. E. O., Knops E., Cords L., Lübke N., Salgado M., Busman-Sahay K., Estes J. D., Huyveneers L. E. P., Perdomo-Celis F., Wittner M. et al. "In-depth virological and immunological characterization of HIV-1 cure after CCR5Δ32/Δ32 allogeneic hematopoietic stem cell transplantation." Nat. Med. (2023); 29: 583–587. doi: 10.1038/s41591-023-02213-x.

[11] "The Global HIV/AIDS Epidemic." HIV.gov, https://www.hiv.gov/hiv-basics/overview/data-and-trends/global-statistics/ (accessed June 13, 2023).

[12] Nowak M. A., May R. M., and Anderson R. M. "The evolutionary dynamics of HIV-1 quasispecies and the development of immunodeficiency disease." AIDS (1990); 4(11): 1095-103. doi: 10.1097/00002030-199011000-00007.

[13] Nowak M. A. and May R. M. "Virus dynamics. Mathematical principles of immunology and virology." Oxford University Press (2000).

[14] Perelson A. S. "Modelling viral and immune system dynamics." Nature Rev. Immunol. (2002); 2: 28–36. doi:10.1038/nri700.

[15] Perelson A. S. and Ribeiro R. M. "Modeling the within-host dynamics of HIV infection." BMC Biol. (2013); 11: 96. doi:10.1186/1741-7007-11-96

[16] Zhang C., Zhou S., Groppelli E., Pellegrino P., Williams I., Borrow P., Chain B. M., and Jolly C. "Hybrid spreading mechanisms and T cell activation shape the dynamics of HIV-1 infection." PLOS Comp. Biol. (2015); 11(4): e1004179. doi:10.1371/journal.pcbi.1004179.

[17] Jolly C., Kashefi K., Hollinshead M., and Sattentau Q. J. "HIV-1 cell to cell transfer across an env-induced, actin-dependent synapse." J. Exp. Med. (2004) 199: 283–293. doi:10.1084/jem.20030648.

[18] Ribeiro R. M., Qin L., Chavez L. L., Li D., Self S. G., and Perelson A. S. "Estimation of the initial viral growth rate and basic reproductive number during acute HIV-1 infection." J. Virol. (2010); 84(12): 6096-6102. doi: 10.1128/JVI.00127-10.

[19] Perelson A. S., Neumann A. U., Markowitz M., Leonard J. M., and Ho D. D. "HIV-1 Dynamics in-Vivo—Virion Clearance Rate, Infected Cell Lifespan, and Viral Generation Time." Science (1996); 271: 1582–1586. doi: 10.1126/science.271.5255.1582.

[20] Westera L., Drylewicz J.,den Braber I., Mugwagwa T., van der Maas I., Kwast L., Volman T., H. R. van de Weg-Schrijver E. H. R., Bartha I., Spierenburg G. et al. "Closing the gap between T-cell life span estimates from stable isotope-labeling studies in mice and humans." Blood (2013); 122(13): 2205–2212. doi: 10.1182/blood-2013-03-488411.

[21] Borghans J. and Ribeiro R. M. "T-cell immunology: the maths of memory." Science (1996); 271: 1582–1586. doi: 10.7554/eLife.26754.

[22] Vrisekoop N., Braber I., Boer A., Ruiter A., Ackermans M., Crabben S., Schrijver E., Spierenburg G., Sauerwein H., Hazenberg M. et al. "Sparse production but preferential incorporation of recently produced naïve T cells in the human peripheral pool." Proc. Natl. Acad. Sci. USA (2008); 105(16): 6115-6120. doi: 10.1073/pnas.0709713105.

[23] Bujoreanu I. and Gupta V. "Anatomy, Lymph Nodes." StatPearls Publishing. https://www.ncbi.nlm.nih.gov/books/NBK557717/ (accessed June 13, 2023).

[24] Ribeiro R. M., Mohri H., Ho D. D., and Perelson A. S. "In vivo dynamics of T cell activation, proliferation, and death in HIV-1 infection: why are CD4+ but not CD8+ T cells depleted?" Proc. Natl. Acad. Sci. USA (2002); 99(24): 15572–15577. doi: 10.1073/pnas.242358099.

[25] Little S. J., McLean A. R., Spina C. A., Richman D. D., and Havlir D. V. "Viral dynamics of acute HIV-1 infection." J. Exp. Med. (1999) 190: 841–850. doi:10.1084/jem.190.6.841.

[26] Korobeinikov, A. "Global properties of basic virus dynamics models." Math Med Biol. 21(2):75-83. (2004). Bull. Math. Biol. (2004); 66(4): 879-883. doi: 10.1016/j.bulm.2004.02.001.

[27] Pantaleo G., Graziosi C., Demarest J. F., Butini L., Montroni M., Fox C. H., Orenstein J. M., Kotler D. P., and Fauci A. S. "HIV infection is active and progressive in lymphoid tissue during the clinically latent stage of disease." Nature (1993); 362(6418): 355-358. doi: 10.1038/362355a0.

[28] Beck S. E., Veenhuis R. T., and Blankson J. N. "Does B Cell Follicle Exclusion of CD8+ T Cells Make Lymph Nodes Sanctuaries of HIV Replication?" Front. Immunol. (2019); 10. doi: 10.3389/fimmu.2019.02362.

[29] Bronnimann M. P., Skinner P. J., and Connick E. "The B-Cell Follicle in HIV Infection: Barrier to a Cure." Front. Immunol. (2018); 9(20). doi: 10.3389/fimmu.2018.00020.

[30] Rezk S. A., Nathwani B. N., Zhao X., and Weiss L. M. "Follicular dendritic cells: origin, function, and different disease-associated patterns." Human Pathology (2013); 44(6): 937-950. doi: 10.1016/j.humpath.2012.10.005.

[31] Uwadiae F. I. "T follicular helper cells." British Society for Immunology, www.immunology.org/public-information/bitesized-immunology/cells/t-follicular-helper-cells (accessed June 13, 2023).

[32] Smith B. A., Gartner S., Liu Y., Perelson A. S., Stilianakis N. I., Keele B. F., Kerkering T. M., Ferreira-Gonzalez A., Szakal A. K., Tew J. G. and Burton G. F. "Persistence of Infectious HIV on Follicular Dendritic Cells." J. Immunol. (2001) 166 (1): 690–696. doi: 10.4049/jimmunol.166.1.690.

[33] Schmitz J., van Lunzen J., Tenner-Racz K., Grossschupff G., Racz P., Schmitz H., Dietrich M., and Hufert F. "Follicular Dendritic Cells (FDC) are Not Productively Infected

with HIV-1 in Vivo." In Vivo Immunol. (1994); Adv. Exp. Med. and Biol. 355: 165–168. doi: 10.1007/978-1-4615-2492-2_28

[34] Burton G. F., Keele B. F., Estes J. D., Thacker T. C., and Gartner S. "Follicular dendritic cell contributions to HIV pathogenesis." Semin. Immunol. (2002); 14(4): 275-84. doi: 10.1016/s1044-5323(02)00060-x.

[35] Heath S. L., Tew J. G., Tew J. G., Szakal A. K., and Burton G. F. "Follicular dendritic cells and human immunodeficiency virus infectivity." Nature (1995); 377(6551): 740-4. doi: 10.1038/377740a0.

[36] Koup R. A., Safrit J. T., Cao Y., Andrews C. A., McLeod G., Borkowsky W., Farthing C., and Ho D. D. "Temporal association of cellular immune responses with the initial control of viremia in primary human immunodeficiency virus type 1 syndrome." J. Virol. (1994); 68(7): 4650-5. doi: 10.1128/JVI.68.7.4650-4655.1994.

[37] Connick E., Mattila T., Folkvord J. M., Schlichtemeier R., Meditz A. L., Ray M. G., McCarter M. D., Mawhinney S., Hage A., White C., and Skinner P.J. "CTL Fail to Accumulate at Sites of HIV-1 Replication in Lymphoid Tissue." J. Immunol. (2007); 178(11): 6975–6983. doi: 10.4049/jimmunol.178.11.6975.

[38] Rivadaneira P. S., Moog C. H., Stan G.-B., Costanza V., Cécile Brunet, Francois Raffi, Ferré V., Mhawej M.-J., Biafore F., Ouattara D. A. et al. "Mathematical modeling of HIV dynamics after antiretroviral therapy initiation: a clinical research study." AIDS Res. Hum Retroviruses (2014); 30(9): 831-4. doi: 10.1089/AID.2013.0286.

[39] Rong L., Gilchrist M. A., Feng Z., and Perelson A. S. "Modeling within-host HIV-1 dynamics and the evolution of drug resistance: trade-offs between viral enzyme function and drug susceptibility." J. Theor. Biol. (2007); 247(4): 804–818. doi: 10.1016/j.jtbi.2007.04.014.

[40] Gadhamsetty S., Beltman J. B., and de Boer R. J. "What do mathematical models tell us about killing rates during HIV-1 infection?" Immunol. Lett. (2015); 168(1): 1-6. doi: 10.1016/j.imlet.2015.07.009.

[41] Akin E., Yeni G., and Perelson A. S. "Continuous and Discrete Modeling of HIV-1 Decline on Therapy." J. Math. Biol. (2020); 81(1): 1-24. doi: 10.1007/s00285-020-01492-z.

[42] Rizal A., Handari B. D., Aldila D., and Rahmayani S. A. "Mathematical models for the dynamics of the HIV with antiretroviral treatment interventions and the effect of apoptosis on T-cells." AIP Conference Proceedings (2020); 2264: 020008. doi: 10.1063/5.0023444.

[43] Fletcher C. V., Staskus K., Wietgrefe S. W., Rothenberger M., Reilly C., Chipman J. G., Beilman G. J., Khoruts A., Thorkelson A., Schmidt et al, T. E. "Persistent HIV-1 replication is associated with lower antiretroviral drug concentrations in lymphatic tissues." Proc. Natl. Acad. Sci. USA. (2014); 111(6): 2307–2312. doi: 10.1073/pnas.1318249111.

[44] Günthard H. F., Wong J. K., Ignacio C. C., Guatelli J. C., Riggs N. L., Havlir D. V., and Richman D. D. "Human immunodeficiency virus replication and genotypic resistance in blood and lymph nodes after a year of potent antiretroviral therapy." J. Virol. (1998); 72: 2422–8. doi: 10.1128/JVI.72.3.2422-2428.1998.

[45] Davenport M. P. and Petravic J. "CD8+ T Cell Control of HIV — A Known Unknown." PLOS Pathog. (2001) 6(1): e1000728. doi: 10.1371/journal.ppat.1000728.

[46] Klatt N. R., Shudo E., Ortiz A. M., Engram J. C., Paiardini M., Lawson B., Miller M. D., Else J., Pandrea I., Estes J. D. et al. "CD8+ Lymphocytes Control Viral Replication in SIVmac239-Infected Rhesus Macaques without Decreasing the Lifespan of Productively Infected Cells." PLOS Pathog. (2010); 6: e1000747. doi: 10.1371/journal.ppat.1000747.

[47] Wong J. K., Strain M. C., Porrata R., Reay E., Sankaran-Walters S., Ignacio C. C., Russell T., Pillai S. K., Looney D. J., and Dandekar S. "In vivo CD8+ T-cell suppression of SIV viremia is not mediated by CTL clearance of productively infected cells." PLOS Pathog. (2010); 6: e1000748. doi: 10.1371/journal.ppat.1000748.

[48] Asquith B., Edwards C. T. T., Lipsitch M., and McLean A. R. "Inefficient Cytotoxic T Lymphocyte–Mediated Killing of HIV-1–Infected Cells In Vivo." PLOS Biol. (2006); 4(4): e90. doi: 10.1371/journal.pbio.0040090.

[49] Wodarz D., Skinner P. J., Levy D. N., and Connick E. "Virus and CTL dynamics in the extrafollicular and follicular tissue compartments in SIV-infected macaques." PLOS Comp. Biol. (2018); 14(10): e1006461. doi: 10.1371/journal.pcbi.1006461.

[50] Nowak M. A. and Bangham C. R. "Population dynamics of immune responses to persistent viruses." Science (1996); 272(5258): 74-9. doi: 10.1126/science.272.5258.74.

[51] Regoes R. R., Barber D. L., Ahmed R., and Antia R. "Estimation of the rate of killing by cytotoxic T lymphocytes in vivo." Proc. Natl. Acad. Sci. USA (2007); 104(5):1599-603. doi: 10.1073/pnas.0508830104.

[52] De Boer R. J., Homann D., and Perelson A. S. "Different dynamics of CD4+ and CD8+ T cell responses during and after acute lymphocytic choriomeningitis virus infection." J. Immunol. (2003); 171(8): 3928–3935. doi: 10.4049/jimmunol.171.8.3928.

[53] Van Deutekom, H. W. M., Wijnker, G., and de Boer, R. J. "The Rate of Immune Escape Vanishes When Multiple Immune Responses Control an HIV Infection." J. Immunol. (2013); 191(6): 3277-3286. doi: 10.4049/jimmunol.1300962.

[54] Perelson A. S. "Modelling viral and immune system dynamics." Nature Rev. Immunol. (2002); 2(1): 28-36. doi: 10.1038/nri700.

[55] Abram M. E., Ferris A. L., Shao W., Alvord W. G., and Hughes S. H. H. "Nature, position, and frequency of mutations made in a single cycle of HIV-1 replication." J. Virol. (2010); 84: 9864–78. doi: 10.1128/JVI.00915-10.

[56] Cuevas J. M., Geller R., Garijo R., López-Aldeguer J., and Sanjuán R. "Extremely High Mutation Rate of HIV-1 In Vivo." PLOS Biol. (2015); 13(9): e1002251. doi: 10.1371/journal.pbio.1002251.

[57] Perelson A. S., Neumann A. U., Markowitz M., Leonard J. M., and Ho D. D. "HIV-1 dynamics in vivo: virion clearance rate, infected cell life-span, and viral generation time." Science (1996); 271(5255): 1582-1586. doi: 10.1126/science.271.5255.1582.

[58] Park E. J., Vujcic L. K., Anand R., Theodore T. S., and Quinnan Jr. G. V. "Mutations in both gp120 and gp41 are responsible for the broad neutralization resistance of variant human immunodeficiency virus type 1 MN to antibodies directed at V3 and non-V3 epitopes." J. Virol. (1998); 72(9): 7099-7107. doi: 10.1128/JVI.72.9.7099-7107.1998.

[59] Ndung'u T. and Weiss R. A. "On HIV diversity." AIDS (2012); 26(10): 1255-60. doi: 10.1097/QAD.0b013e32835461b5.

[60] Saad-Roy C. M., Morris S. E., Metcalf C. J. E., Mina M. J., Baker R. E., Farrar J., Holmes E. C., Pybus O. G., Graham A. L., Levin S. A. et al. "Epidemiological and evolutionary considerations of SARS-CoV-2 vaccine dosing regimes." Science (2021); 372(6540): 363-370. doi: 10.1126/science.abg8663.

[61] Roberts H. E., Hurst J., Robinson N., Brown H., Flanagan P., Vass L., Fidler S., Weber J., Babiker A., Phillips R. E. et al. "Structured Observations Reveal Slow HIV-1 CTL Escape." PLOS Genetics (2015); 11(2): e1004914. doi: 10.1371/journal.pgen.1004914.

[62] Doekes, H. M., Fraser C., and Lythgoe K. A. "Effect of the Latent Reservoir on the Evolution of HIV at the Within- and Between-Host Levels." PLOS Comp. Biol. (2017) 13(1): e1005228. doi:10.1371/journal.pcbi.1005228.

[63] Davenport, M. P., Loh L., Petravic J., and Kent S. J. "Rates of HIV immune escape and reversion: implications for vaccination." Trends Microbiol. (2008); 16(12): 561-566. doi:/10.1016/j.tim.2008.09.001.

[64] Fabreti L. G., Castro D., Gorzoni B., Janini L. M. R., Antoneli F. "Stochastic Modeling and Simulation of Viral Evolution." Bull Math Biol. 2019 Apr;81(4):1031-1069. (2019) doi: 10.1007/s11538-018-00550-4.

[65] Read, E. L. et al. "Stochastic effects are important in intrahost HIV evolution even when viral loads are high." PNAS (2012); 109(48): 19727-19732. doi:10.1073/pnas.1206940109.

[66] Gillespie, D. T. "Exact Stochastic Simulation of Coupled Chemical Reactions." J. Phys. Chem. (1977); 81(25): 2340–2361. doi:10.1021/j100540a008.

[67] Farhang-Sardroodi S. et al. "The effect of spatial randomness on the average fixation time of mutants." PLOS Comp. Biol. (2017); 13(11): e1005864. doi: 10.1371/journal.pcbi.1005864.

[68] Kimura M. "On the Probability of Fixation of Mutant Genes in a Population." Genetics (1962); 47(6): 713–719. doi: 10.1093/genetics/47.6.713.

[69] Haldane J. "A mathematical theory of natural and artificial selection, part V: selection and mutation." Math. Proc. Camb. Phil. Soc. (1927); 23(7): 838–844. doi: 10.1017/S0305004100015644

[70] Wright S. "Evolution in Mendelian populations." Genetics (1931); 16(2): 97–159. doi: 10.1093/genetics/16.2.97.

[71] Fisher R. A. "The evolution of dominance in certain polymorphic species." The American Naturalist (1930); 64(694): 385–406. doi: 10.1086/280325.

[72] Moran P. A. P. "Random processes in genetics". Math Proc. Camb. Phil. Soc. (1958); 54(1): 60–71. doi:10.1017/S0305004100033193.

[73] Nowak M. A. "Evolutionary Dynamics: Exploring the Equations of Life." Belknap Press (2006); 93-105.

[74] Gokhale C. S., Papkou A., Traulsen A., and Schulenburg H. "Lotka–Volterra dynamics kills the Red Queen: population size fluctuations and associated stochasticity dramatically change host-parasite coevolution." BMC Evol. Biol. (2013); 13: 254. doi: 10.1186/1471-2148-13-254.

[75] Ewens W. "The probability of survival of a new mutant in a fluctuating environment." Heredity (1967); 22: 438–443. doi: 10.1038/hdy.1967.53.

[76] Otto S. P. and Whitlock M. C. "The probability of fixation in populations of changing size." Genetics (1997); 146(2): 723-33. doi: 10.1093/genetics/146.2.723.

[77] Parsons T. L. and Quince C. "Fixation in haploid populations exhibiting density dependence II: The quasi-neutral case." J. Theor. Pop. Biol. (2007); 72(4): 468–479. doi: 10.1016/j.tpb.2007.04.002.

[78] Berke G. "The binding and lysis of target cells by cytotoxic lymphocytes: Molecular and cellular aspects." Annu. Rev. Immunol. (1994); 12(1): 735-773. doi: 10.1146/annurev.iy.12.040194.003511.

[79] Slatkin M. "Fixation Probabilities and Fixation Times in a Subdivided Population." Evolution (1981); 35(3): 477-488. doi: 10.2307/2408196.

[80] Pattni K., Broom M., Rychtář J. and Silvers L. J. "Evolutionary graph theory revisited: when is an evolutionary process equivalent to the Moran process?" Proc. R. Soc. A. (2015); 471: 20150334. doi: 10.1098/rspa.2015.0334.

[81] Voorhees B. "Birth–death fixation probabilities for structured populations." Proc. R. Soc. A. (2012); 469: 20120248. doi: 10.1098/rspa.2012.0248.

[82] Whitlock M. C. "Fixation probability and time in subdivided populations." Genetics (2003); 164(2): 767–779. doi: 10.1093/genetics/164.2.767.